Sustainable Energy & Fuels

Interdisciplinary research for the development of sustainable energy technologies

Accepted Manuscript

This article can be cited before page numbers have been issued, to do this please use: A. Radwan, T. Katsura, S. Memon, E. Abo-Zahhad, O. M. Abdelrehim, A. Serageldin, M. Elmarghany, A. Khater and K. Nagano, *Sustainable Energy Fuels*, 2020, DOI: 10.1039/D0SE01102A.

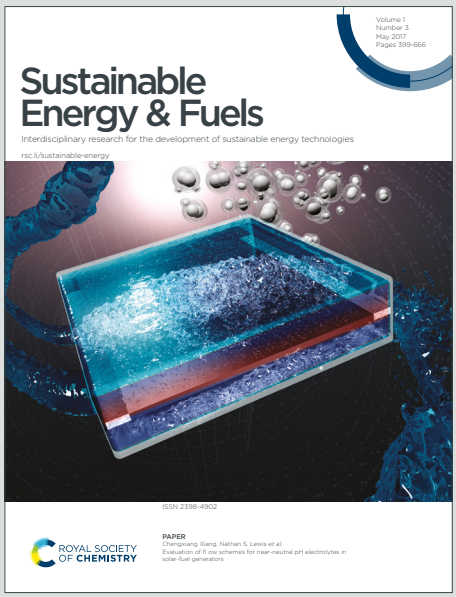

ROYAL SOCIETY OF CHEMISTRY

rsc.li/sustainable-energy

Development of a new vacuum-based photovoltaic/thermal collector, thermal and exergy analyses

Ali Radwan[1,4,5]*, Takao Katsura[1], Saim Memon[2], Essam M. Abo-Zahhad[3], O. Abdelrehim[4,5], Ahmed A. Serageldin[1], Mohamed R. Elmarghany[4,5], Asmaa Khater[4,5], Katsunori Nagano[1]

[1]Division of Human Environmental Systems, Faculty of Engineering, Hokkaido University, N13-W8, Kita-ku, Sapporo 060-8628, Japan.

[2]London Centre for Energy Engineering, Division of Electrical and Electronic Engineering, School of Engineering, London South Bank University, 103 Borough Road, London, SE1 0AA, UK.

[3]Mechanical Power Engineering Department, Faculty of Energy Engineering, Aswan University, Aswan 81528, Egypt.

[4]Mechanical Power Engineering Department, Faculty of Engineering, Mansoura University, El Mansoura 35516, Egypt

[5]Mansoura University Nanotechnology Center, Mansoura University, El-Mansoura, 35516, Egypt

*Corresponding Author: Ali Radwan
Position: - Postdoctoral fellow, Faculty of Engineering, Hokkaido University
Address: Division of Human Environmental Systems, Faculty of Engineering, Hokkaido University, N13-W8, Kita-ku, Sapporo 060-8628, Japan
Email: ali.radwan@ejust.edu.eg
Tel: +81-070-4158-4708

View Article Online
DOI: 10.1039/D0SE01102A

Abstract

Photovoltaic-thermal (PV/T) solar collectors convert solar radiation into electrical power and heat. A considerable amount of received solar energy can be lost to the ambient from the top surface of the PV/T module, especially in windy regions. Thus, in this study, a new vacuum-based photovoltaic thermal (VPV/T) collector is designed and comparatively analyzed with the conventional PV/T collector. The new design differs from the conventional PV/T design by including vacuum layer above the silicon wafer. Besides, to enhance the heat dissipation from the silicon wafer in the VPV/T design to the thermal absorber, the thicknesses of ethylene-vinyl acetate and tedlar polyester tedlar layers underneath the silicon wafer are decreased. A comprehensive 3D conjugate thermal model is developed and validated. The comparison is conducted at steady and transient conditions. The effect of Reynolds number (Re), wind speed, glass emissivity, and vacuum pressure are investigated. And finally, the exergy analysis for both designs are compared. The results showed that the new VPV/T collector has accomplished a 26.6% increase in the thermal power without changing the electrical power gain at Re of 50 and solar irradiance of 1000Wm^{-2}. In addition, the vacuum pressure degradation from 0.01 Pa to 10 Pa slightly decreases the gained thermal power of the new VPV/T. A further increase in the vacuum pressure from 10 Pa to 1.013×10^5 Pa significantly decreases the gained thermal power with a slight increase in the electrical power. Furthermore, the total predicted VPV/T and the conventional PV/T exergy efficiency are 40% and 32%, respectively.

Keywords: - Photovoltaic thermal; vacuum photovoltaic thermal; exergy analysis; vacuum pressure; conjugate heat transfer.

View Article Online
DOI: 10.1039/D0SE01102A

1. Introduction

Solar thermal energy is the most popular renewable source of energy [1]. Approximately 3.85 million Exajoule of energy is received from the sun and absorbed by the Earth annually [2]. The solar radiation can by harnessed with two main techniques: i) solar electricity generation using photovoltaic (PV) technology [3] and ii) solar thermal systems using solar thermal collectors. Both techniques are exploited the sun's rays, on a small- or large-scale solar parks. The PV/Thermal (PV/T) systems simultaneously generate electricity and thermal energy[4] [5]. The thermal energy is gained through the cooling of the PV [6]. Therefore, the overall conversion efficiency of the PV/T system can be improved. Hence, the PV/T consists of PV module attached to a thermal absorber. The PV/T systems are utilized for domestic heating and electricity supply. Sultan and Efzan [7] extensively reviewed the recent PV/ T advances and applications. However, a further improvement in the overall conversion efficiency must be done.

Enhancing the performance of the PV/T systems has been focused on improving the PV electrical performance or the thermal heat gain by the cooling fluid or both [8]. Pang et al. [9] performed a comprehensive analysis on the performance of PV/T regarding the working fluid, geometry, and terrestrial conditions. Fuentes et al. [10] experimentally compared the commercial pure PV and the PV/T system. They reported an overall conversion efficiency (thermal and electrical) for the PV/T system up to 80%.

The main challenge in the PV/T systems is to enhance the usability of the existing source of energy in a reliable and effective way. Several studies compared different operating conditions and working fluids for the PV/T collectors [7]. Numerous review papers considered the application of nanofluid for PV/T systems [11,12]. Khanjari et al. [13] numerically studied the performance of Ag and Alumina nanofluids and compared it with the base fluid (water). The influence of the nanoparticle loading ratio and coolant velocity on the thermal and electrical performance was considered and exergy analysis was performed. They reported that both the energy and exergy efficiencies were enhanced by increasing the nanoparticle loading. Sardarabadi et al. [14] studied the consequence of utilizing SiO_2 nanofluid water based in PV/T system. The total conversion efficiency with 1 wt.% and 3 wt.% nanofluids were improved by 3.6% and 7.9%, respectively.

Recent advancements led to modify the structure of the PV/T system for improving the overall performance. Hassani et al. [15] theoretically evaluated the life cycle exergy of PV/T for three different system configurations. In their work, water and Ag/water nanofluids were employed as optical filters. They proved that using the optical filter provided a substantial quantity of thermal energy. Ahmed and Radwan [16] used a nanocomposite to modify the PV structure in the PV/T system. Higher heat dissipation from PV was reported with higher system efficiency. Sopian et al. [17] studied an improved PV/T system design with double passes of air. The double-pass PV/T showed superior overall performance compared to single-pass PV/T. Nahar et al. [18] introduced an innovative PV/T system by excluding the absorber plate. Consequently, the thermal part was attached directly to the rear side of the PV module by thermal grease. The performance of the PV/T system under different operating conditions was evaluated. The data showed that the overall efficiency of the new system reaches 84.4%.

Based on the literature, the PV/T technology has many potentials for a broad application as it generates electricity and thermal energy with high overall performances. Moreover, the PV/T has the benefit of a limited carbon footprint in comparison with the two separated PV systems and thermal collectors. However, it is evident that the PV/T is not a mature technology yet. The prior literature was mainly directed to two main ways. First, they focused on finding an optimal PV cooling method. Second, the researchers were focused on enhancing the structure of the PV materials for higher electrical efficiency.

In the recent PV/T investigations, the backside of the thermal absorber was isolated to increase the thermal energy. However, the heat loss from the top surface of the PV/T module can be a dominant factor, especially in the windy regions with higher solar radiations whilst moderate or lower ambient temperatures. In these weather conditions, a substantial amount of heat can be lost to the atmosphere from the upward surface of the PV/T. And due to the transparency requirements of the top PV/T surface, no conventional opaque thermal insulation can be utilized. Furthermore, the conventional structure of the polycrystalline PV module has two layers of EVA and TPT. These two layers located underneath the silicon wafer and cause an increase in the PV module temperature and lower heat dissipation to the water in the thermal absorber. Consequently, a significant decrease in system total efficiency.

Therefore, this study focuses on decreasing the thermal energy loss from the top surfaces of the PV modules in the PV/T systems. This target can be attained by utilizing a vacuum layer

View Article Online
DOI: 10.1039/D0SE01102A

above the PV module. This idea reduces the heat loss from the top surface of the PV module. Besides, using a low-emissive coated layer on the inner glass cover side could further decrease the radiative heat loss. Therefore, a higher thermal efficiency can be accomplished. It is worth mentioning that the new approach could lead to slight reduction in the gained electrical power. Therefore, the conventional layers of the most polycrystalline PV cell are adjusted. The proposed VPV/T collector is compared with the conventional design of the PV/T collector at the same conditions. Hence, a comprehensive 3D conjugate heat transfer model with detailed exergy analyses are developed. The model is validated with the researcher's results in the literature. The steady-state, transient, exergy analyses for both designs are compared at different operating conditions. Furthermore, the effect of vacuum pressure on the thermal performance of the VPV/T design is estimated.

2. Physical model

In this study, the conventional PV/T and the new VPV/T systems are presented in Fig. 1, and Fig. 2 respectively. In the conventional PV/T design, the PV module is attached to a thermal absorber. This thermal absorber is used to regulate the module temperature using pure water as a circulating fluid. The PV module contains glass layer, top EVA layer, silicon wafer, bottom EVA layer and finally a TPT layer with thicknesses of 3mm, 0.5mm, 0.2mm, 0.5mm, and 0.3mm, respectively [19]. The silicon layer generates electricity and it is surrounded by transparent EVA layer to protect it and accomplish electrical insulation [20]. The EVA and TPT layers have thermal conductivities of 0.311 W/mK and 0.15 W/mK, respectively which cause significant decrease in the heat transfer to the water in the thermal absorber [19]. Besides, it results in a higher PV cell temperature and lower heat gain and high thermal energy loss compared to other systems. The higher cell temperature, the lower gained electric power, and less lifetime. Furthermore, in the windy regions, the thermal energy loss to the atmosphere from the PV top surface decreases the system thermal efficiency.

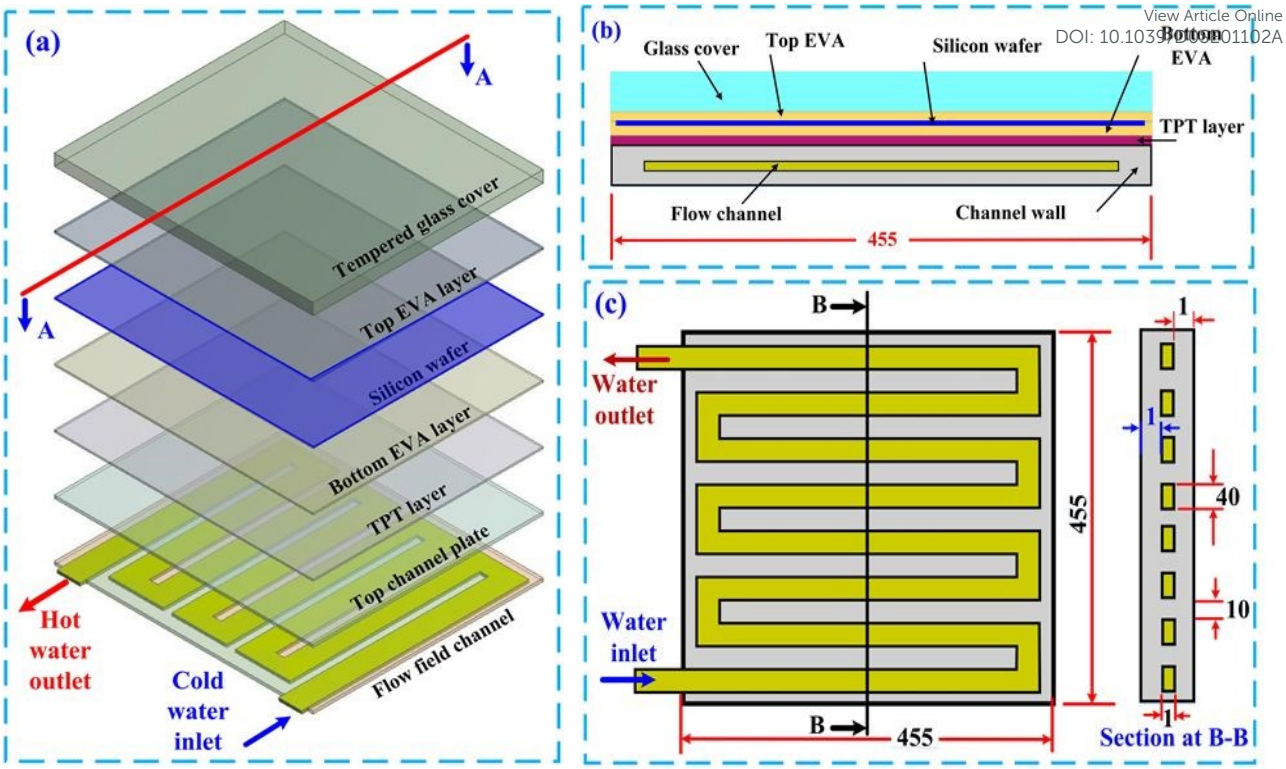

Fig. 1 Detailed structure of the conventional PV/T module (a) layers structure; (b) cross-section at A-A; and (c) flow filed design in the thermal absorber.

The modified VPV/T module is illustrated in Fig. 2. The two main differences between the conventional PV/T and the VPV/T designs are the vacuum layer above the silicon wafer and different EVA layer thickness . t The 0.3 mm thickness vacuum layer is used to decrease the heat loss from the top surface of the silicon wafer, especially in the windy regions. In addition, this allows the increase in the thermal heat gain in the VPV/T design. However, this vacuum layer could result in a higher photovoltaic module operating temperature in the VPV/T design and decreases the gained electrical power. To avoid this risk, a high heat dissipation rate from the silicon wafer to the cooling water should be achieved. Therefore, the thermal resistance for EVA and the TPT layer underneath the silicon wafer should be decreased. This forces the heat generated in the silicon wafer due to the solar radiation absorption to rapidly dissipate to the water in the thermal absorber. Recently, the first author of this paper investigated two different methods to accomplish this target. The first method involved the use of a nano-composite EVA layer underneath the silicon layer. In addition, the TPT layer was replaced with an aluminium tedlar sheet. The nano-composite layer included doping the boron nitride nanoparticles in the EVA matrix [16]. This enhances the conduction heat transfer through the EVA layer underneath the silicon wafer without affecting the light characteristics and the electrical insulation characteristics. The second method is decreasing the thickness of this layer from 0.5 mm to

View Article Online
DOI: 10.1039/D0SE01102A

0.2mm [19]. The later thickness is commercially available in the markets for this application and cost-effective compared to the larger thickness. Also, the smaller thickness decreases the thermal resistances at the backside. The second method is most effective compared to the first one. Therefore, it has been applied to this work.

The composited edge sealed vacuum insulated glazed enclosure is proposed to keep the vacuum pressure for longer life without performance degradation. An array of pillars made of stainless-steel with a diameter of 6 mm and spaced at 50 mm are used to sustain the vacuum gap and prevent glass breakage. These dimensions are attained based on the real fabrication for a vacuum-based solar thermal collector in [21]. The module area used in the present study is 455×455 mm^2. The composite edge seal of 10 mm for vacuum enclosure utilized was the invention of Dr Memon that ultrasonically soldered the primary seal, at low-temperature around 200°C, made of composite CS-186 or Sn-Pb-Zn-Sb-AlTiSiCu in the proportion ratio of 56:39:3:1:1 by wt% and the secondary seal made of reinforced steel epoxy [22–24]. This 10 mm wide composite edge sealed vacuum glazing integrated in the VPV/T module. Therefore, the active PV area in both designs is around 455×455 mm^2. This area includes the cross-sectional area of 7×7 support pillars spaced at 50 mm. The edge sealing with 10 mm in the VPV/T is considered as EVA interval to avoid the silicon wafer fracture at the sides in the PV/T design. Therefore, the solar cell area in both designs are nearly the same (with neglecting the pillars effect in the VPV/T design). Serpentine flow field with channel height and width of 1 mm and 50 mm respectively is used for cooling the PV in both the PV/T and the VPV/T modules. Aluminum channel with 1 mm wall thickness and 5 mm separation between each flow channel is used for the thermal absorber. Table 1 shows the detailed dimensions of the PV/T and the VPV/T systems along with the thermophysical properties of each layer are depicted in Table1.

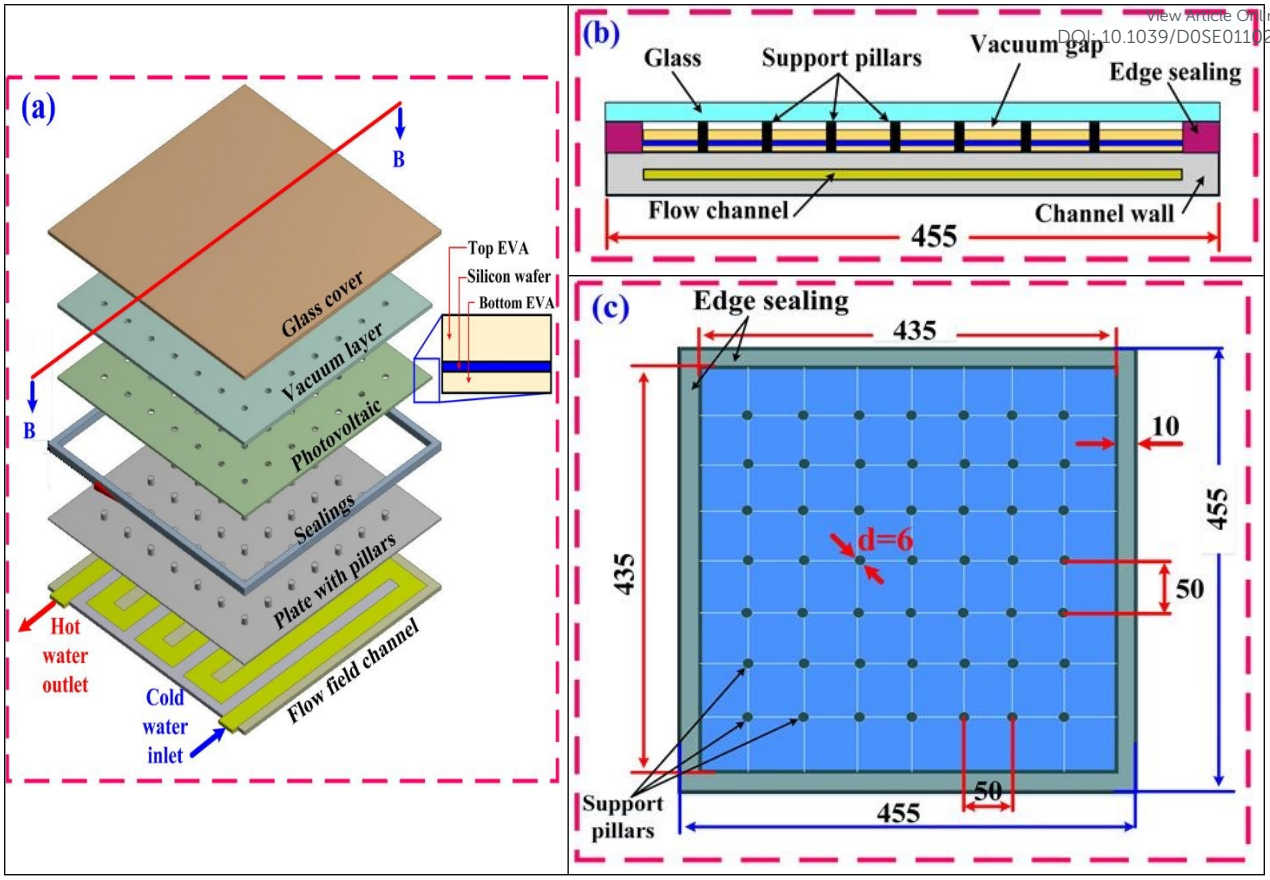

Fig. 2 Detailed structure of the new VPV/T module (a) layers structure; (b) cross-section at B-B; and (c) plane view to show the support pillars location.

Table 1 PV/T and VPV/T modules dimensions and properties.

Layers	Detailed dimensions (mm)		Properties		
	PV/T module	VPV/T module	ρ (kg/m^3)	C_p (J/kg.K)	k (W/m.K)
Tempered glass cover	3	3	3000	500	2
Vacuum layer	---	0.3	---	---	Equ. (11)
Top EVA	0.5	0.5	960	2090	0.311
Silicon wafer	0.2	0.2	2330	677	130
Bottom EVA	0.5	0.2	960	2090	0.311
Tedlar	0.3	---	1200	1250	0.15
Aluminum channel	1	1	2179	871	202.4
Fluid layer	1	1	Ref. [25]	Ref. [25]	Ref. [25]

View Article Online
DOI: 10.1039/D0SE01102A

3. Theoretical analysis

In the present analysis, the complete computational domains shown in Fig.1 and Fig. 2 are modelled. In the PV/T and VPV/T systems, the received solar radiation is partially absorbed, transmitted, and reflected based on the optical properties of each layer. In the incident, solar radiation on the glass cover is partially absorbed and mostly transmitted to the top EVA layer due to the higher transparency of the cover. The absorbed part causes an increase in the glass cover temperature while the transmitted part is partially absorbed by the top EVA and mostly transmitted to the silicon wafer due to the higher transparency of the top EVA layer. Also, the absorbed portion increases the top EVA temperature. The transmitted solar radiation from the top EVA is mostly (around 98%) absorbed in the silicon wafer. This absorbed part is partially converted to electricity, (around 20% at solar cell reference conditions), in the silicon wafer and the remaining is converted to heat. The portion converted to heat increases the cell temperature and declines the electrical efficiency. To keep a safe PV operating temperature, an efficient thermal management technique should be applied.

In the proposed design, conduction, convection, and radiation heat exchanges should be simultaneously considered. The following assumptions are adopted.

1. The solid domains are considered as homogeneous and their properties were temperature independent.
2. The contact resistance resulted from the attachment of the module components are neglected.
3. The PV/T and VPV/T modules back sides are completely isolated to achieve the maximum benefit of thermal energy for domestic hot water supply.
4. The flow in the mini-scale serpentine channel thermal absorber is assumed to be laminar, maximum used Reynolds number is 150, and incompressible.
5. Temperature-dependent water properties are assumed considered as higher order polynomial equations in Ref. [25].

The unsteady three-dimensional energy equation form the solid layers is represented as follows [26]:

$$\rho c_p\left(\frac{\partial T}{\partial t}\right) = k_i\left(\frac{\partial^2 T}{\partial x^2} + \frac{\partial^2 T}{\partial y^2} + \frac{\partial^2 T}{\partial z^2}\right) + q_i \quad (1)$$

where k_i, T_i and q_i are the thermal conductivity, elemental temperature, and the heat generation term, respectively. The heat generation is considered due to the absorption of solar

View Article Online
DOI: 10.1039/D0SE01102A

radiation in the glass, top EVA, and the silicon wafer. The heat generation in the layers below the silicon wafer is neglected due to the low transparency of silicon wafer. Therefore, Eq. (1) is solved for all the solid domains, including the edge sealing, pillars aluminium channel materials. The values of q_i in the glass, top EVA, and silicon layer are calculated by Eq. (2), (3) and (4), respectively. The absorptivity, reflectivity, and transmittivity of each layer are presented in Table 2.

For glass layer: $q_g = \frac{G \cdot \alpha_g \cdot A_g}{V_g}$ (2)

For top EVA layer: $q_{Eva,\ top} = \frac{G \cdot \alpha_{Eva} \cdot \tau_g \cdot A_{Eva}}{V_{Eva}}$ (3)

For silicon layer: $q_{sc} = \frac{(1-\eta_{sc}) \cdot G \cdot \alpha_{sc} \cdot \tau_{eva} \cdot \tau_g \cdot A_{sc}}{V_{sc}}$ (4)

Where V is the layer volume, A is the surface area of the layer and G is the solar radiation falling on top surface of the module. The cell electrical efficiency is expressed as follows [27]:

$$\eta_{sc} = \eta_{ref}(1 - \beta_{ref}(T_{sc} - T_{ref})) \quad (5)$$

Where: η_{ref} is the PV efficiency at standard temperature T_{ref} of 25 ^{o}C. And T_{sc} is the solar cell operating temperature. For the thermal modelling of the PV/T and VPV/T modules, equation (5) is used to estimate the cell efficiency as a function of silicon wafer temperature. The PV specifications at standard testing conditions (STC) for crystalline silicon solar cells are a typical reference efficiency of 20% (AM1.5) at a reference temperature of T_{ref}= 298 K with β_{ref} of 0.0045 K^{-1} [28]. These parameters were used as the same for both PV/T and VPV/T to clarifies the effect of vacuum layer addition. Based on Eq. (4) and (5), the term q_{sc} depends on the electrical efficiency of the cell. This efficiency is function of the PV module temperature. And this operating temperature is also a function of the internal heat generation in the silicon wafer. Therefore, to solve this problem, an iterative technique is applied. The details of this iterative technique are explained in the author's earlier work [16].

View Article Online
DOI: 10.1039/D0SE01102A

Table 2: PV layers reflectivity (R), absorptivity(α), and transmissivity(τ), and emissivity (ε) as detailed presented in [29].

Layer	**(R)**	**(α)**	**(τ)**	**(ε)**
Glass	0.04	0.04	0.92	0.85
EVA	0.02	0.08	0.90	
Silicon	0.08	0.90	0.02	
TPT	0.86	0.128	0.012	0.9
Aluminium	---	----	----	0.9

For the fluid domain in the mini-scale serpentine thermal heat absorber, the governing equations of the unsteady, laminar flow, and incompressible can be written as follows:

Continuity equation:

$$\frac{\partial \rho U}{\partial x} + \frac{\partial \rho V}{\partial y} + \frac{\partial \rho W}{\partial z} = 0 \quad (6)$$

Momentum equations in x, y, and z directions:

$$\frac{\partial \rho U}{\partial t} + U\frac{\partial \rho U}{\partial x} + V\frac{\partial \rho U}{\partial y} + W\frac{\partial \rho U}{\partial z} = -\frac{\partial p}{\partial x} + \mu\left(\frac{\partial^2 U}{\partial x^2} + \frac{\partial^2 U}{\partial y^2} + \frac{\partial^2 U}{\partial z^2}\right) \quad (7)$$

$$\frac{\partial \rho V}{\partial t} + U\frac{\partial \rho V}{\partial x} + V\frac{\partial \rho V}{\partial y} + W\frac{\partial \rho V}{\partial z} = -\frac{\partial p}{\partial y} + \mu\left(\frac{\partial^2 V}{\partial x^2} + \frac{\partial^2 V}{\partial y^2} + \frac{\partial^2 V}{\partial z^2}\right) \quad (8)$$

$$\frac{\partial \rho W}{\partial t} + U\frac{\partial \rho W}{\partial x} + V\frac{\partial \rho W}{\partial y} + W\frac{\partial \rho W}{\partial z} = -\frac{\partial p}{\partial z} + \mu\left(\frac{\partial^2 W}{\partial x^2} + \frac{\partial^2 W}{\partial y^2} + \frac{\partial^2 W}{\partial z^2}\right) \quad (9)$$

Energy equation:

The fluid energy equation expressed in the following form

$$\frac{\partial \rho C_p T}{\partial t} + U\frac{\partial \rho C_p T}{\partial x} + V\frac{\partial \rho C_p T}{\partial y} + W\frac{\partial \rho C_p T}{\partial z} = k\left(\frac{\partial^2 T}{\partial x^2} + \frac{\partial^2 T}{\partial y^2} + \frac{\partial^2 T}{\partial z^2}\right) \quad (10)$$

Where ρ, μ , $\mathrm{U}, \mathrm{V}, \mathrm{W}$ and P are water density, viscosity, the velocities in x, y, and z, and the coolant pressure, respectively.

Surface to surface (S2S) model is used to account the radiation process in the vacuum gap as in [30]. In this region, the heat exchange between the top surface of the EVA layer and the bottom surface of the glass layer mostly occurs with radiation, especially at low pressure as explained in [21,31]. This model considers the emissivity effect and the view factor in the

View Article Online
DOI: 10.1039/D0SE01102A

calculations. The view factors are automatically estimated from the model dimensions and ordinations from the computational domain geometry. Therefore, the heat exchange is mostly occurred by radiation through the vacuum and by conduction in support pillars and the edge sealing. The gas conduction effect can be neglected if the internal pressure is less than 0.1 Pa [32]. In this work, the gas thermal conductivity is considered as a function of the pressure, as shown in Eq. (11). The inner surface of the tempered glass cover is assumed to have emissivity of 0.18 as usually used in vacuum glazing. The vacuum layer thermal conductivity is estimated as flows [33]:-

$$k_{vacuum} = \frac{k_o}{1 + \frac{(1.07 \times 10^{-4}) \times T}{l_{vacuum} \times P}} \quad (11)$$

Where T is the absolute average temperature between the two sides of the vacuum layer, l_{vaccum} is the vacuum gap thickness (0.0003 m in this study), and P is the vacuum pressure in Pa. Besides, k_o is the reference air conductivity (0.026 W/mK). The S2S model details exist in ANSYS theory guide [30].

To investigate the effect of vacuum pressure on the module temperature, equation (11) is used to estimate the vacuum layer thermal conductivity as a function of the vacuum pressure and vacuum gap average temperature. The vacuum layer thermal conductivity increases with increasing the vacuum pressure at the same vacuum gap thickness and vacuum temperature. This estimated thermal conductivity is updated for the vacuum layer at each simulation and then all governing equations are iteratively solved until reaching the convergence criteria.

3.1. Module characterization

To compare the performance of each design at a specific operating condition, several characterization parameters are used. The electrical PV power is estimated using: -

$$P_{el} = \eta_{sc} \cdot G \cdot \alpha_{sc}.\tau_{top}.A_{sc} \quad (12)$$

Where the electrical efficiency, η_{sc} , is estimated as by Equ. (5). And G, α_{sc}, A_{sc} are the received solar radiation by the collector, solar cell absorptivity, PV module packing factor, and solar cell area, respectively. The solar radiation receiving area which occupied by the solar cell is about 0.188 m^2 and 0.189 m^2 for the PV/T and VPV/T system, respectively. This small difference has resulted from the area occupied by 49 support pillars.

The cooling heat sink attached to the photovoltaic thermal collector consumes a pumping power to overcome the friction. The friction power is estimated as follows: -

View Article Online
DOI: 10.1039/D0SE01102A

$$P_{friction} = \left(\frac{\dot{m}}{\rho_w}\right) \times \Delta P \quad (13)$$

Where $\dot{m}$, and ΔP are the coolant flow rate and the pressure drop in the thermal absorber, respectively. The net gained electric power generated by the PV module is estimated as follows:-

$$P_{net} = P_{el} - P_{friction} \quad (14)$$

The thermal heat gained by the collector can be estimated as follows:-

$$P_{th} = \dot{m} \cdot C_{p,w} \cdot (T_{out} - T_{in}) \quad (15)$$

Where T_{out} and T_{in} are the water outlet and inlet temperatures, respectively. The module thermal efficiency can also be estimated as follows [35]:-

$$\eta_{th} = \frac{\dot{m} \cdot C_{p,w} \cdot (T_{out} - T_{in})}{G \cdot A_{sc}} \quad (16)$$

The heat loss from the top surface of the VPV/T and PV/T modules are estimated using the following equation: -

$$Q_{th,loss} = h_w.A_g.(T_g - T_a) + \varepsilon_g.\sigma.A_g.(T_g^4 - T_s^4) \quad (17)$$

Where h_w, A_g, T_g, T_a, ε_g, and T_s are the heat transfer coefficient caused due to the wind effect in (W/m^2.K), glass area in (m^2), glass temperature in (K), ambient temperature in (K), glass external emissivity, and sky temperature in (K), respectively.

The term h_w is estimated using the correlation as follows [36].

$$h_w = 5.7 + 3.8 \times U_w \quad (18)$$

Where U_w is the wind speed in m/s. Based on Eq. (18), it is evident that increasing the wind speed significantly increases the convection heat transfer coefficient from the top surface of the PV module. Hence, it could influence the thermal performance of both designs. Therefore, the performance of both systems is compared at a wide range of wind speed up to 6 m/s.

The simulation is conducted at various values of inlet water velocities. And the results are depicted as a function of flow Reynolds number expressed as flows: -

$$Re = \frac{\rho V_{in} D_h}{\mu} \quad \text{and} \quad D_h = \frac{4(W_{ch} \times H_{ch})}{2(W_{ch} + H_{ch})} \quad (19)$$

Where V_{in} and D_h are the water velocity normal to the inlet section and channel hydraulic diameter, respectively.

View Article Online
DOI: 10.1039/D0SE01102A

3.2. Exergy assessments

Exergy assessment is used to estimate the exergy losses and estimate the total system exergy efficiency. The electrical energy (Ex_{el}) is considered as pure exergy [37,38]. The thermal exergy (Ex_{th}) is estimated as follows [37,39]:-

$$Ex_{th} = \underbrace{\dot{m}_f \cdot C_f \cdot (T_{f,out} - T_{f,in})}_{thermal\ power} \cdot \underbrace{\left(1 - \frac{T_a}{T_{f,out}}\right)}_{carnot\ factor} \quad (20)$$

$T_{f,in}$ and $T_{f,out}$ are the coolant inlet and outlet temperatures, respectively. The Carnot factor is also expressed as a function of T_m. The term T_m is calculated by [37]:

$$T_m = \frac{h_{out} - h_{in}}{S_{out} - S_{in}} = \frac{(T_{f,out} - T_{f,in})}{\ln\left[\frac{T_{f,out}}{T_{f,in}}\right]} \quad (21)$$

Then, the term Ex_{th} is expressed as follows: -

$$Ex_{th} = \underbrace{\dot{m}_f \cdot C_f \cdot (T_{f,out} - T_{f,in})}_{thermal\ power} \cdot \underbrace{\left(1 - \frac{T_0}{T_m}\right)}_{carnot\ factor} \quad (22)$$

The coefficient of radiation exergy (Ψ_s) is used to calculate the exergy gain from the solar radiation. Ψ_s is described as follows [40]:

$$\Psi_s = 1 - \frac{T_a}{T_{sun}} \quad (23)$$

The term T_{sun} is the sun solar radiation temperature of 6000 K [1]. At that point, the solar radiation rate of exergy per unit surface area (e_{sol}) is estimated as follows: -

$$e_{sol} = \Psi_s \cdot G \quad (24)$$

Hence, the electrical, thermal, and total exergy efficiency ξ_{el}, ξ_{th}, and ξ are calculated by equations (25), (26) and (27), respectively:

$$\xi_{el} = \frac{Ex_{el}}{\Psi_s \cdot G \cdot A} \quad (25)$$

$$\xi_{th}(t) = \frac{Ex_{th}}{\Psi_s \cdot G \cdot A} \quad (26)$$

$$\xi(t) = \frac{Ex_{el} + Ex_{th}}{\Psi_s \cdot G \cdot A} \quad (27)$$

View Article Online
DOI: 10.1039/D0SE01102A

The climatological parameters are considered variable with the time for the transient simulation. While for the steady-state conditions, these values are considered constant corresponding to each simulated case.

3.3. Boundary conditions

Steady-state and transient boundary conditions of the PV/T and VPV/T system are applied as two different conditions. In the steady-state, uniform water velocity with a temperature of 30°C is assumed at the inlet of the thermal absorber for both designs. The heat generation in each layer of the PV/T and VPV/T system was estimated at fixed solar radiation of 1000 W/m^2 . The values of the coolant velocities are changed according to a flow Reynolds number ranging from 10 to 150. Zero pressure is defined at absorber outlet. Heat loss by convection and radiation is applied at the top surface. Thermal coupled boundary conditions are used to share the temperatures and heat fluxes on the interfaces between every two consequent layers. Furthermore, the no-slip conditions are considered for faces between the fluid and solid regions. Finally, adiabatic boundary condition is taken at the sides and the back side of the thermal absorber to attain the highest possible thermal energy gain. This assumption can be experimentally confirmed by efficient thermal insulation. In the transient boundary condition, a typical summer day with variable weather conditions is taken to compare the collector's performance in Cairo, Egypt (30.0444° N, 31.2357° E) on 10th of July 2019. These conditions are applied as transient profiles.

3.4. Mesh independence test

Before conducting the simulation work, mesh independent test is performed for both the conventional PV/T and new VPV/T designs at Reynolds number of 10 and 150. This test confirmed that the extracted results are not affected by changing the number of elements. Generally, it is noticed that changing the number of elements slightly changes the gained thermal energy. However, increasing the number of elements to 1.36 and 1.23 million for the PV/T and the VPV/T systems respectively changes the predicted pressure drop. And further increasing the number of elements beyond these values slightly influences the anticipated results of the pressure drop and gained thermal energy. However, this increase in the number of elements increases the computational time. Therefore, these number of elements are adopted to simulate the two cases of the PV/T and the VPV/T systems.

View Article Online
DOI: 10.1039/D0SE01102A

Table 3 mesh test for (a) conventional PV/T and (b) new VPV/T system

	(a) Conventional PV/T					(b) New VPV/T			
	Re= 10		Re= 150			Re= 10		Re= 150	
No. of elements (million)	ΔP (Pa)	Q_{th} (W)	ΔP (Pa)	Q_{th} (W)	No. of elements (million)	ΔP (Pa)	Q_{th} (W)	ΔP (Pa)	Q_{th} (W)
1.75	197.8	32.2	3032.7	110.09	1.62	197.71	61.74	3031.8	122.4
1.36*	**197.3**	**32.2**	**3025.4**	**110.09**	**1.23***	**197.32**	**61.83**	**3025.5**	**122.4**
1.03	194.3	32.2	2977.9	110.09	0.99	195.50	61.83	2996.6	122.4
0.63	183.4	32.2	2811.7	110.10	0.79	187.65	61.84	2877.2	122.4
0.21	176.0	32.3	2703.8	110.12	0.18	175.95	64.10	2703.8	122.6

*Selected number of elements.

3.5. Model validation

The developed thermal model is validated in several pieces of research conducted by the author [41]. Additionally, the predicted results of this simulation are compared with experiments of [42] and numerical work of [43]. During the validation, the current model is modified to simulate the same problems in [42] and [43] with the same dimensions, flow conditions, and meteorological conditions. Figure 3 shows the predicted results of PV temperature, coolant outlet temperature, and PV electrical power in Fig. 3a, Fig. 3b and Fig. 3c, respectively. A high accuracy is observed with a maximum relative deviation from the results in [42] around 3.3 %, 1.6 % and 2.4 % for the estimated PV temperature, coolant outlet temperature, and generated PV electrical power, respectively.

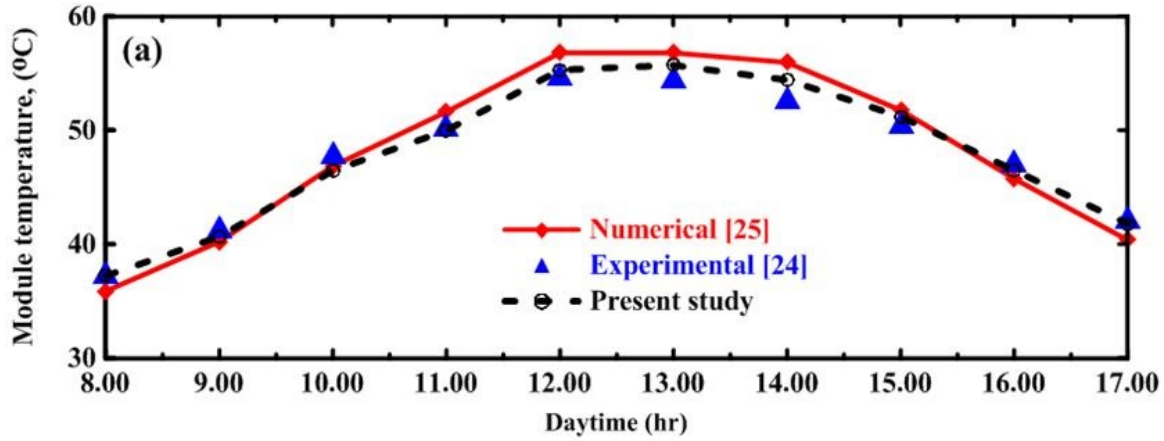

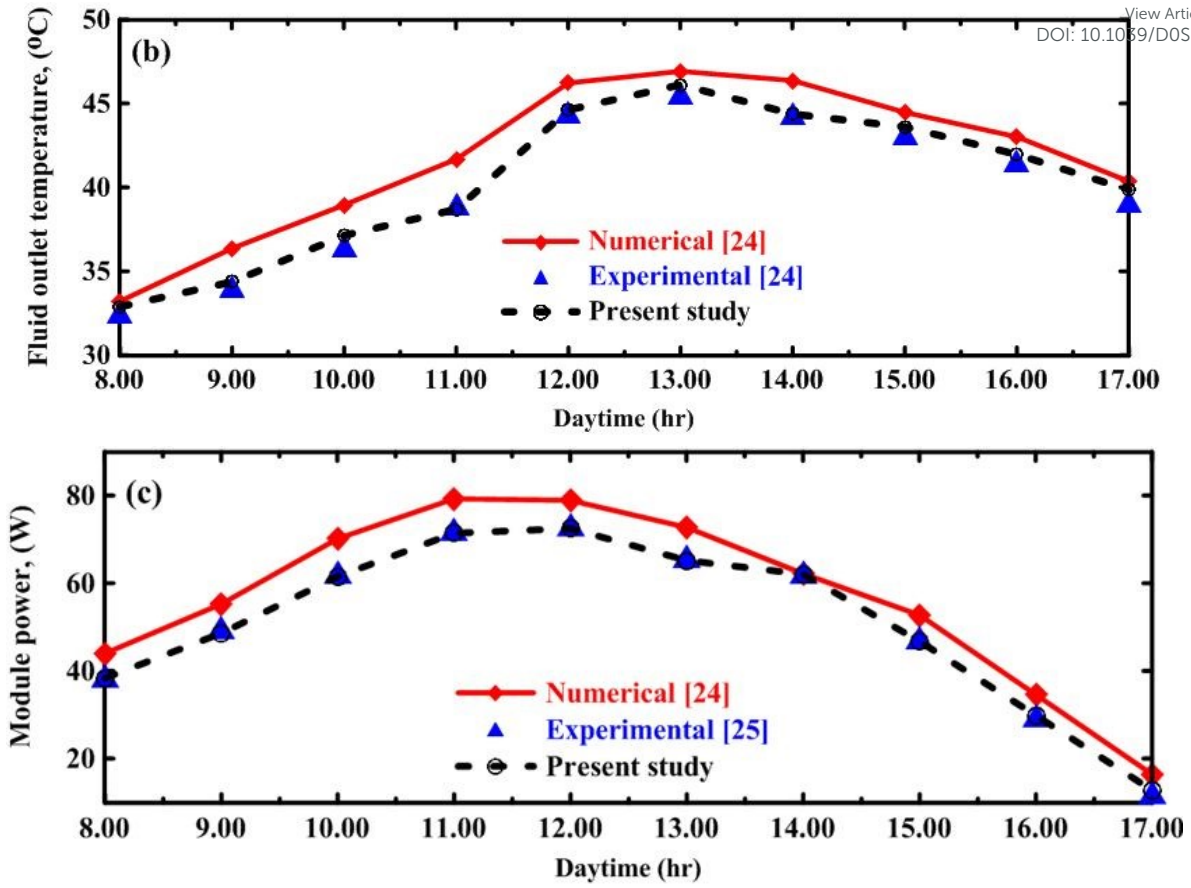

Fig. 3 Validation of the current predicted (a) PV temperature, (b) coolant outlet temperature, and (c) PV generated electrical power by comparison with the experiments in [42] and numerical values in [43].

The flow length in the last serpentine turn has a length of around 420 mm. Therefore, the ratio of the flow length and the flow channel hydraulic diameter is 210 mm. Thus, fully developed flow can be considered. For a rectangular cross-sectional channel, the fully developed analytical velocity profile for a channel with aspect ratio of 50, the maximum velocity locates at the channel centre with a magnitude of 1.5 times the inlet mean velocity [44]. For all the simulated results, the ratio between the maximum outlet velocity and the uniform inlet velocity is checked and found to be around 1.496 times of the inlet mean velocity.

4. Results and Discussion

The results section is divided into five subsections. In section 4.1, the effect of changing the water flow rate on the performance of conventional PV/T and the new VPV/T system is presented. Section 4.2 presents a comparison between both systems under different wind speed conditions. Section 4.3 describes the effect of different design parameters such as the emissivity

View Article Online
DOI: 10.1039/D0SE01102A

of surfaces facing the vacuum gap and the effect of vacuum pressure on the thermal analysis of the vacuum VPV/T system. Section 4.4 describes the transient comparison of the new VPV/T system and the conventional PV/T system. Finally, detailed exergy analyses for both numerically validated designed models are presented at section 4.5.

4.1. Effect of flow rate

Fig. 4 shows the comparative analysis of composite edge sealed VPV/T collector with the conventional PV/T collector at different cooling water flow rates and a constant value of solar irradiance (G) of 1000 W/m^2, vacuum pressure (P) of 0.01 Pa, ambient temperature (T_a) of 30 ^{o}C, and wind speed (U_w) of 2 m/s as an example. The variation of average silicon layer temperature with the flow rates is represented in Fig. 4a. It can be seen that, at low values of water flow rate, the PV temperature is higher by 20 ^{o}C when the VPV/T system is applied, and this is due to the vacuum gap which reduces the amount of heat loss through the glass thus the cell temperature increased. The difference in cell temperature between both systems decreases with the increase in the water flow rate. This is due to the increase of the convective heat transfer coefficient accompanying the increase of Reynolds number. It is worth mentioning that, with the increase in the flow Re number more than 50 achieves relatively the same PV temperature while the coolant outlet temperature for the VPV/T is much higher. This clarifies that for the new VPV/T system, the same electrical power can be generated with higher heat gain at this Re number.

The maximum PV temperature has the similar trend as the average cell temperature. For instance, in Fig. 4b at Re=10, VPV/T predicts maximum solar cell temperature of 30 ^{o}C which is higher than the PV/T collector system. Fig. 4c shows the variation of the top glass surface temperature with Re. The glass temperature decreases by increasing of Re and becomes lower when the VPV/T system is employed for all values of Re. This is due to the insulation implemented by the air gap, which prevents the heat from moving towards the glass wall and force it to move through the bottom EVA layer. The result of this effect can also be seen in Fig. 4d that represents the water outlet temperature at various Re. As the heat is forced to move through the EVA layer to the cooling water, the temperature of water increases when VPV/T is used compared to PV/T system. This is also due to the width reduction of EVA layer.

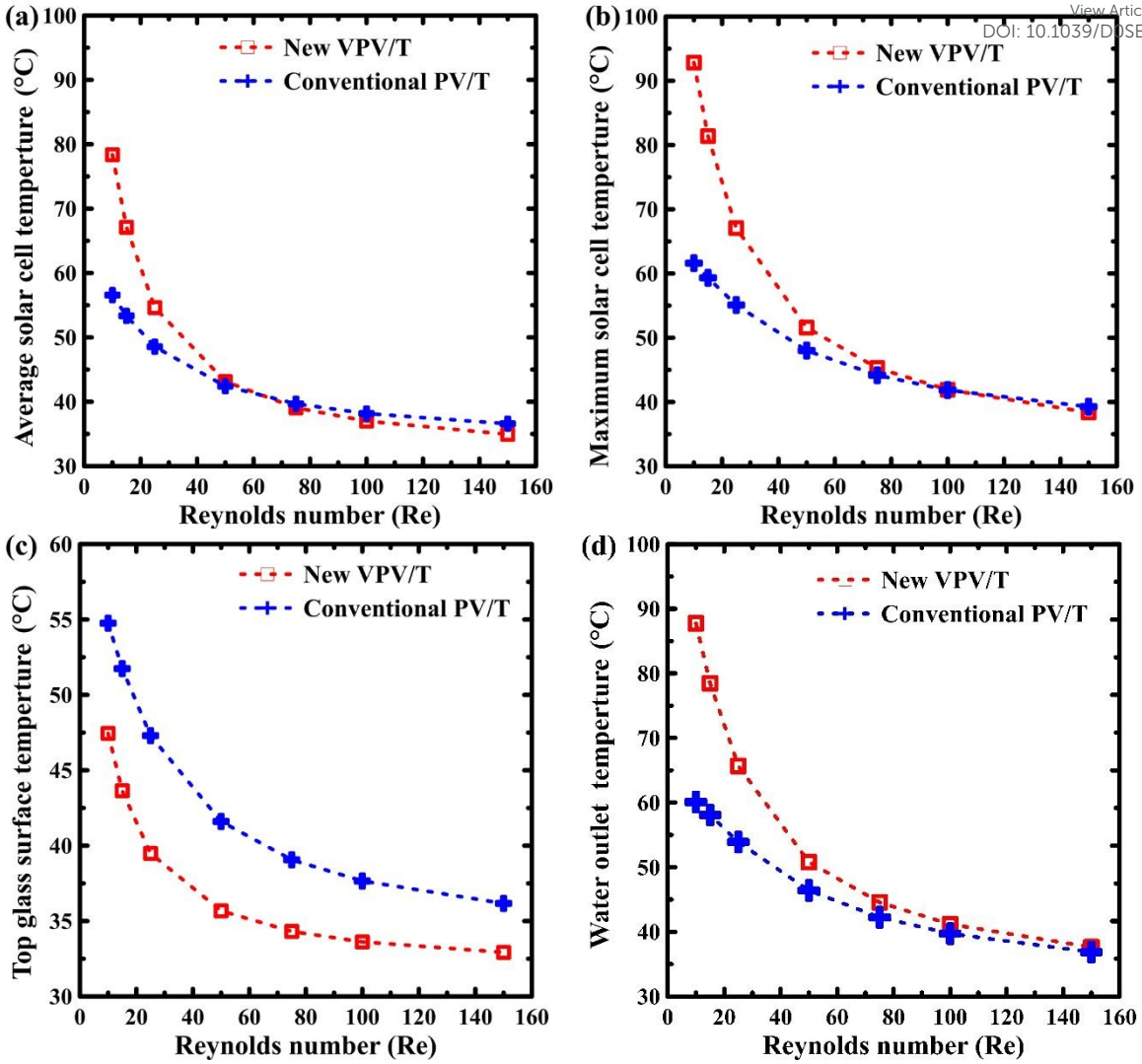

Fig. 4 Assessment of VPV/T and PV/T for a) average PV temperature, b) maximum PV tempreature, c) top glass surface temperature, and d) cooling water outlet temperature

The variation of gained thermal power, collector top surface heat loss, and the gained heat gain versus Re are depicted in Fig. 5. The gained thermal power, calculated by Eq. (15), increased with an increase of mass flow rate, $\dot{m}$ and outlet temperature, T_{out}. It can be seen from Fig. 5a, at the same Re, thermal heat gained is higher when the VPV/T is used compared to PV/T system due to the increase of water outlet temperature resulted from lower heat loss. Heat loss from the PV system depends on the convection and radiation from the top glass layer to the surroundings as seen in Eq. (17). Fig 5b shows the variation of heat loss versus Re. At the same conditions, VPV/T shows a reduction in the heat loss compared to conventional PV/T system, and this is due to the decrease of the top glass temperature because of the vacuum gap.

The water cooling is attained using pump. To estimate the power consumption by this pump, the friction power is estimated. In addition, The variation of the photovoltaic cell net gained with Re is shown in Fig. 5c. The photovoltaic net gained power estimated as the difference between

the photovoltaic power and friction power consumed by the pump for the same module area and estimated by Equ. (14). From the calculated data, the ratio of the friction power consumed by the pump to the generated electrical power represents a maximum of 0.03% at Re of 150 for the conventional PV/T. The friction power is very small and nearly the same for both PV/T and VPV/T designs because of the same flow conditions and heat sink design are used.

Moreover, the conventional PV system gives higher solar cell power gained compared to vacuum VPV/T system at lower Re. This is because, for the same value of solar radiation, cell power gained depends on cell efficiency which decreases with the increase of cell temperature that is lower in the case of conventional PV/T system. However, increasing the Re number up to around 70, no significant difference in the electrical gained power can be depicted. This means that at higher Re, the VPV/T collectors favourable compared to the PV/T collector because of the accomplishment of higher thermal energy gain.

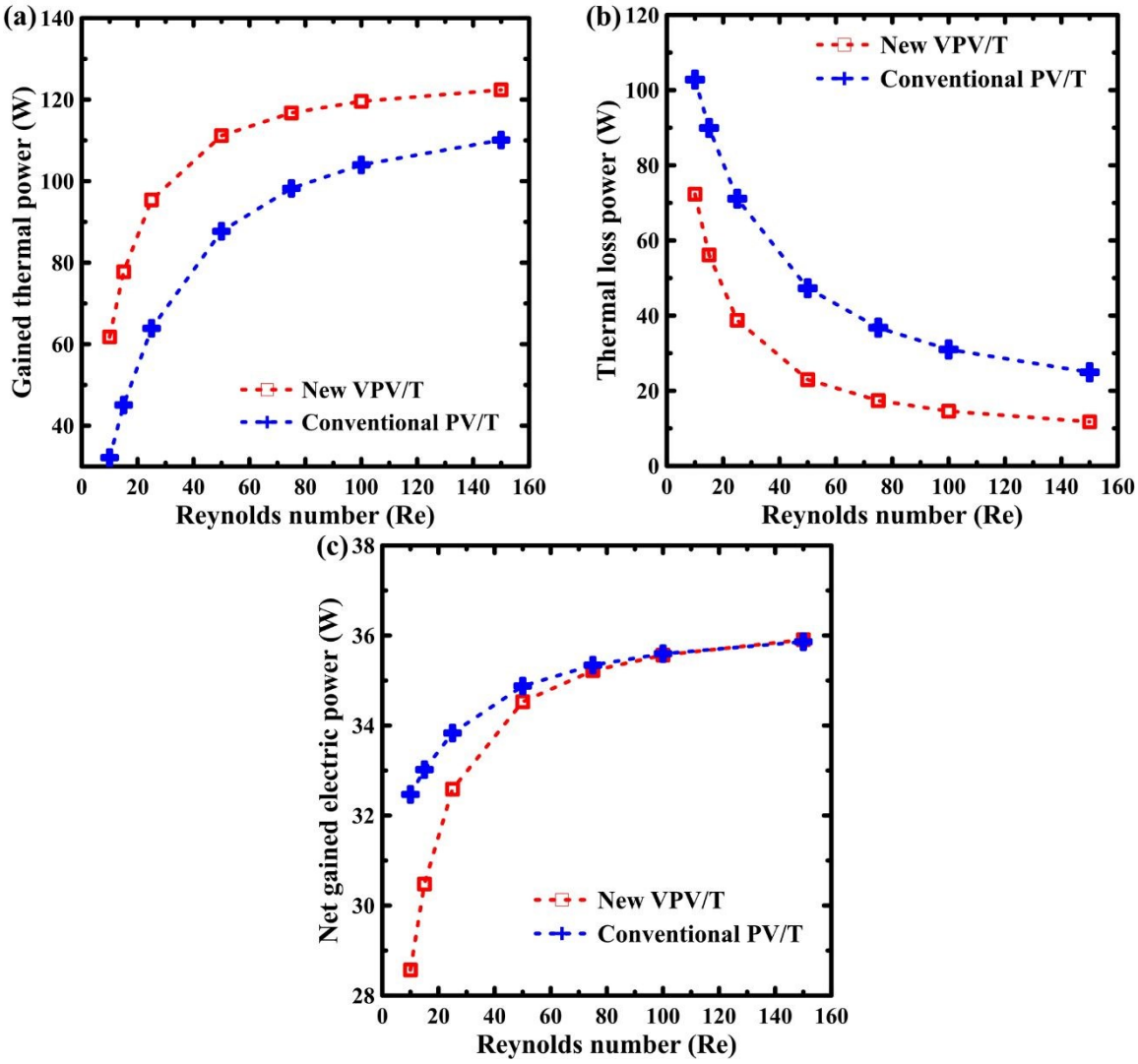

Fig. 5 Influence of a) thermal heat gain, b) heat loss power, and c) cell net gain at different Re

View Article Online
DOI: 10.1039/D0SE01102A

The local temperature distribution provides an indication of the system performance and thermal stresses. Therefore, the temperature distributions of the top glass layer for the new VPV/T system and the conventional PV/T system are presented in Fig.6 with dynamic values of Re. As can be seen in Fig. 6, when conventional PV/T is used, the local temperature is lower at the left top corner at the cooling water inlet and increases along with the top glass cover and reaches its highest value at the right top corner near the water outlet. When the VPV/T system is employed, the temperature is distributed uniformly along with the cell with higher values around the edges due to the edge sealing made by indium sealing and at the supported stainless-steel pillars. This thermal bridge caused by pillars and edge sealing results in a large percentage of heat loss in the VPV/T to surface. This amount of heat loss can be decreased in the large area collectors with lower conductive edge sealing and ultra-fine pillars. The local temperature declines with the increase of Re. At Re of 10, the maximum and minimum detected temperatures are 55 °C and 34 °C, respectively. It is found that increasing Re to 150 decreases the maximum and minimum observed temperature to 40 °C and 30 °C, respectively.

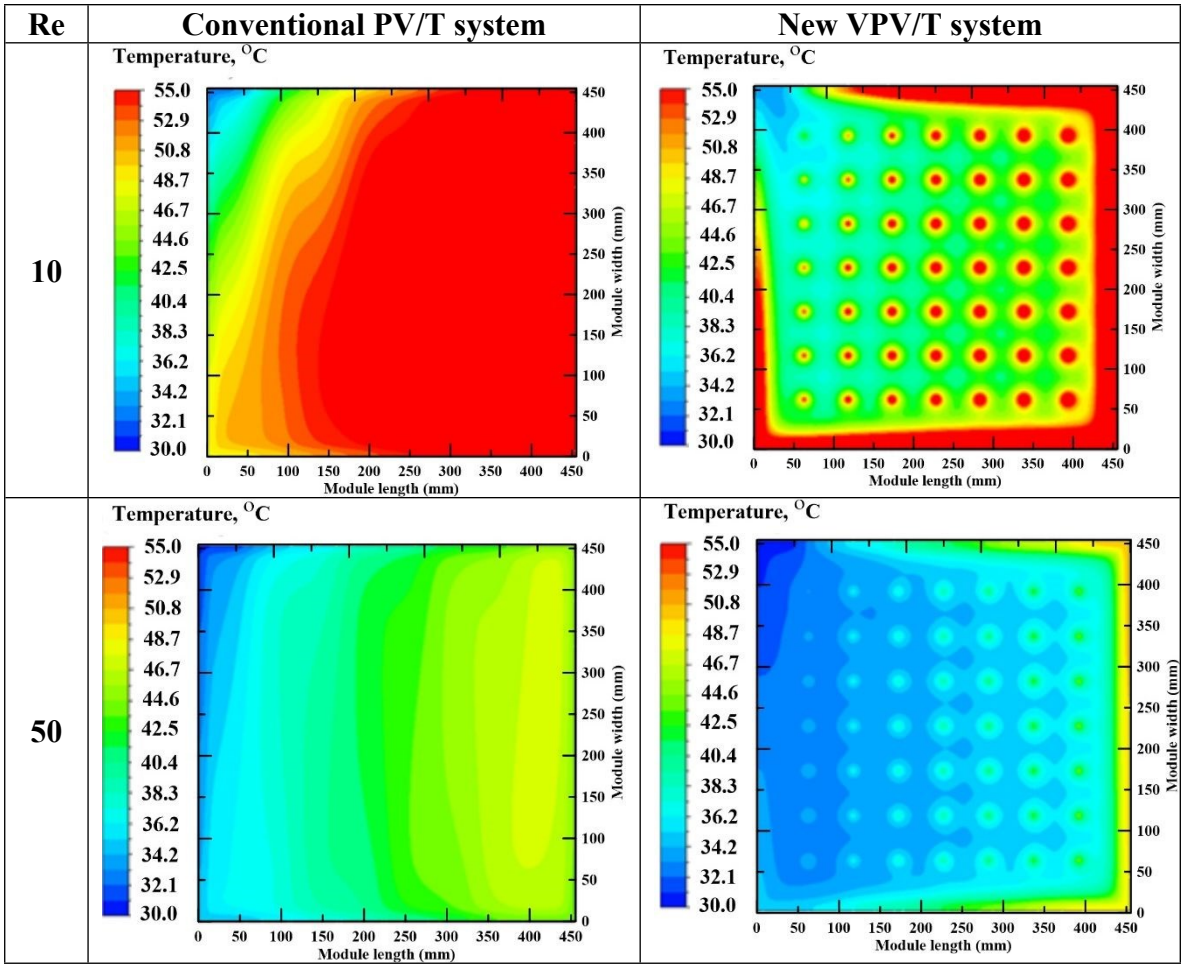

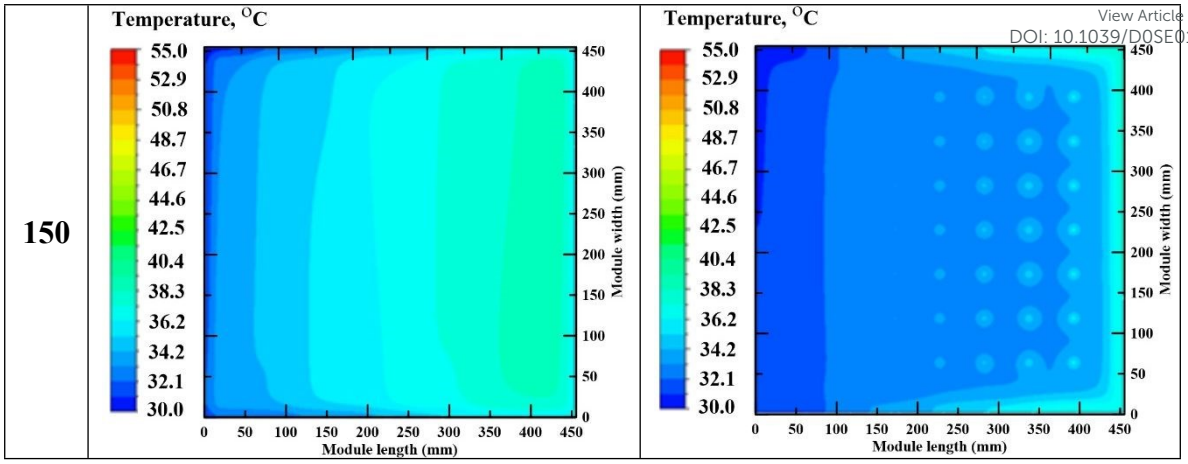

Fig. 6. Local top glass surface temperature for PV at different values of Re.

4.2. Effect of wind speed

The effect of wind speed on the performance of VPV/T system compared with conventional PV/T system is discussed at Re of 10, G =1000 W/m^2 and cavity vacuum pressure of 0.01 Pa. The effect of wind speed on the average solar cell, maximum solar cell, top glass, and outlet water temperatures is shown in Fig. 7. It can be seen from Fig. 7a and Fig. 7b that the average solar cell temperature and maximum solar cell temperature decrease with the increase of wind speed, as the heat transfer losses increase through the glass layer. Conventional PV/T system shows higher average solar cell temperature compared to the new VPV/T system. Top glass surface temperature is dependent on the convection heat transfer coefficient of the surrounding air, it increases with an increase of wind speed leading to a decrease in the top glass surface temperature. Fig. 7d shows the variation of cooling water outlet temperature with wind speed. Cooling fluid outlet temperature declines with the increase of wind speed as the thermal power decreases. It is worth mentioning that, increasing wind speed significantly decreases all these parameters. Whilst these parameters are slightly affected by the wind speed in the VPV/T system. This verifies that the proposed VPV/T system provides stable output parameters at different wind speeds.

View Article Online
DOI: 10.1039/D0SE01102A

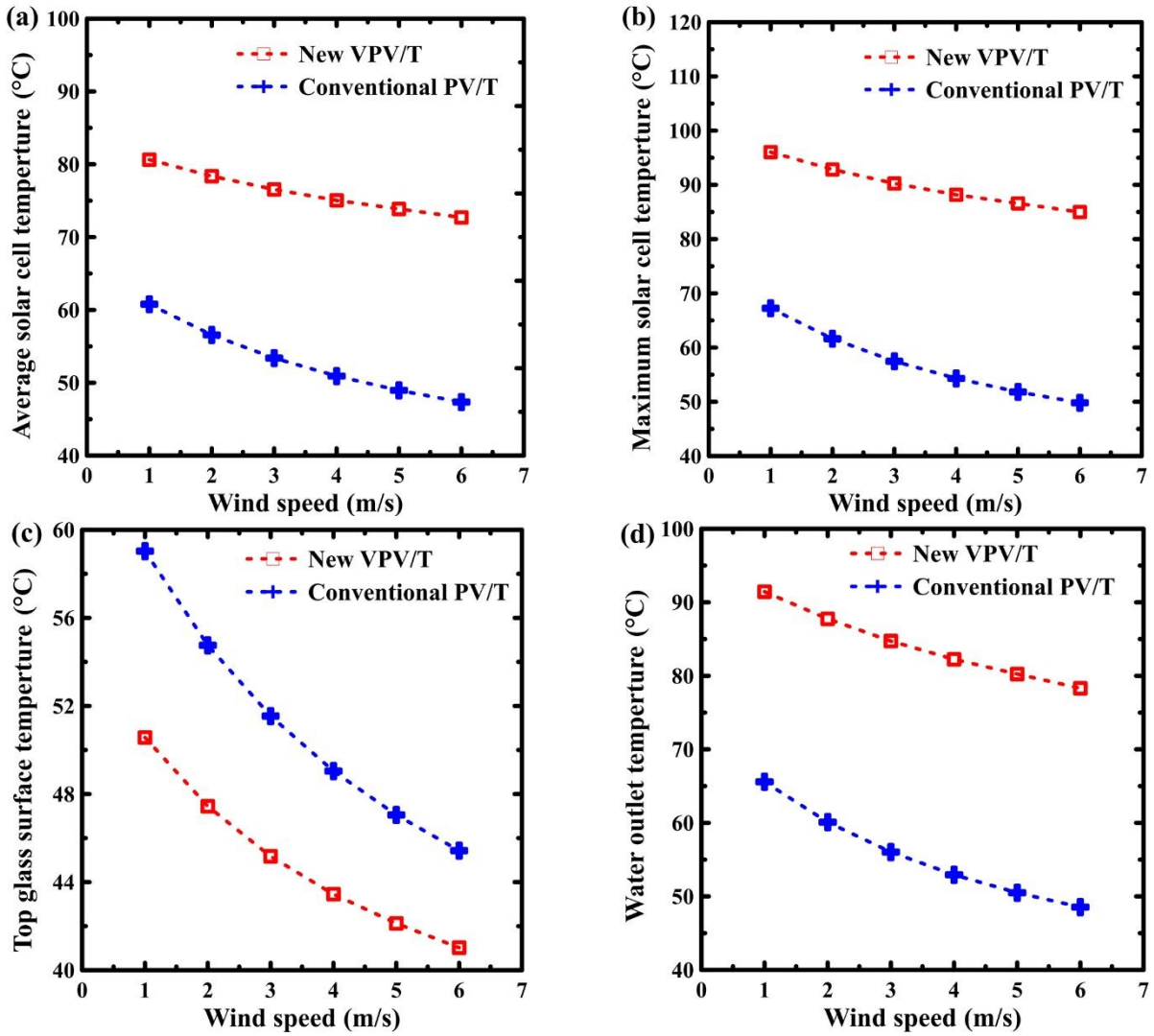

Fig. 7 Comparison between VPV/T and PV/T for a) average PV temperature, b) maximum PV tempreature, c) top glass surface temperature, and d) water outlet temperature at different wind speed.

Figure 8 shows the impact of wind speed on the gained thermal power, heat loss, and photovoltaic cell net gained at Re of 10, G of 1000 W/m^2 and cavity vacuum pressure of 0.01 Pa. From Fig. 8a, the gained thermal power decreases with increasing the wind speed as the water outlet temperature decreases. The gained thermal power is higher when the VPV/T system is used compared to conventional PV/T system. The heat loss increases with the wind speed, as depicted in Fig. 8b. Conventional PV/T system shows higher heat loss compared to new VPV/T system. Fig. 8c indicates the variation of the photovoltaic cell net gained, P_{el}, calculated from Eq. (12), at various wind speeds. The cell net gained power increases with the increase of wind speed as it depends on the solar cell efficiency that increases with the decrease of the solar cell temperature. Conventional PV/T system shows higher values of photovoltaic cell net gained

View Article Online
DOI: 10.1039/D0SE01102A

compared to VPV/T system. Furthermore, at a wind speed of 1 m/s, Re of 10 and G of 1000W/m^2, the generated electric power is around 32 W and 28 W for the conventional PV/T and the new VPV/T systems, respectively. A total 12.5% of reduction in the generated electric power with the new VPV/T collector system. Whilst the thermal heat gain increased from 39 W to 68 W for the conventional PV/T and the new VPV/T systems, respectively. An increase of total 74% in the thermal heat gain is accomplished by using the new VPV/T system. The heat loss at this condition of lower Re is higher than the heat gain and much dominant in the conventional PV/T system. For instance, the heat loss is around 96 W and 67 W for the conventional PV/T and the new VPV/T system, respectively. This higher heat loss is attributed to the lower Re number of 10 through this simulated part.

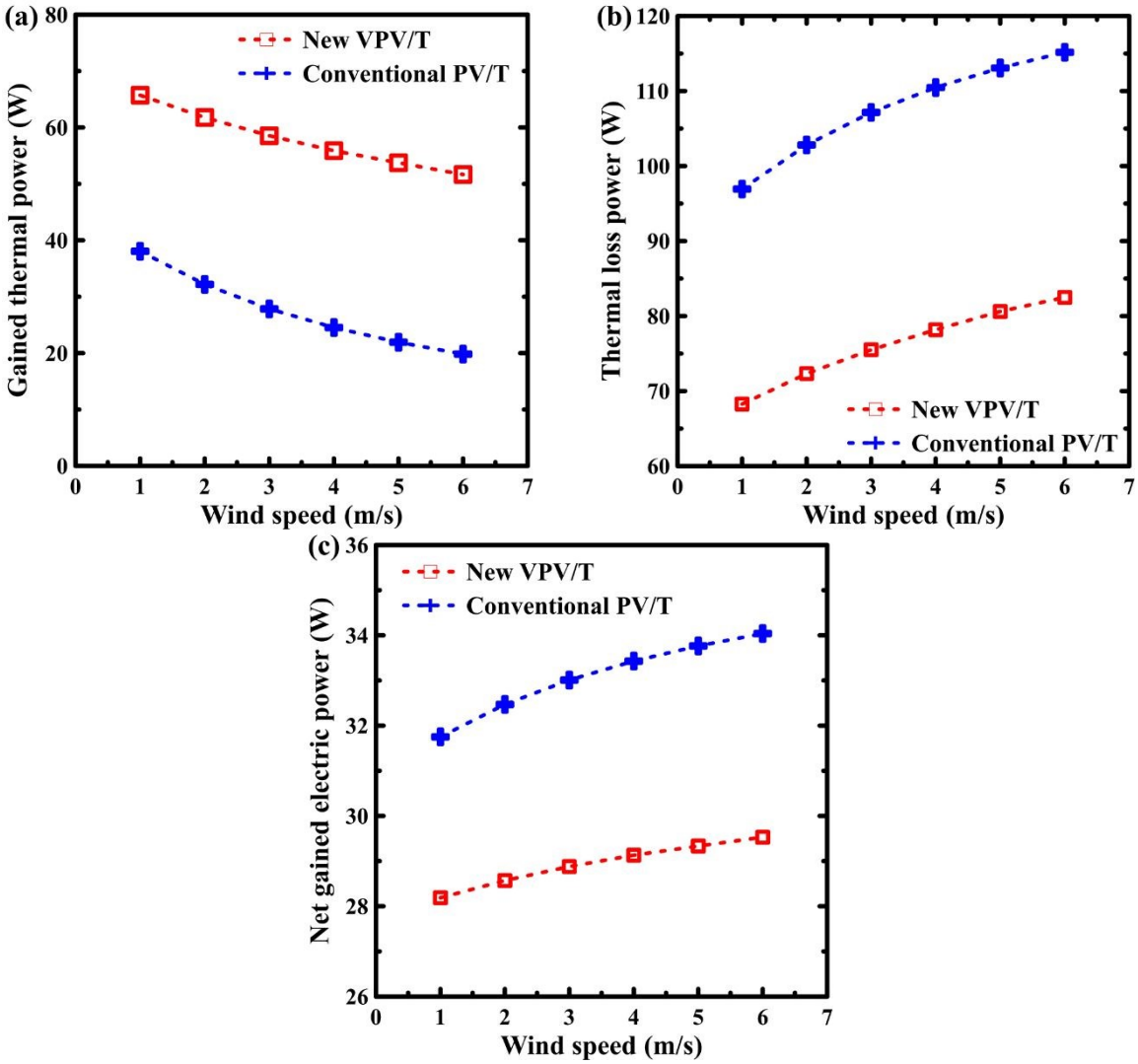

Fig. 8 Variation of a) thermal heat gain, b) heat loss power, and c) cell net gain at different wind speed

The wind speed effect on the local temperature distribution of the top glass surface is illustrated in Fig. 9 at Re of 10. At U_w=1 m/s and with conventional PV/T system, the maximum

View Article Online
DOI: 10.1039/D0SE01102A

temperature is located at the outlet of the cooling channel where the minimum temperature located at the cooling water inlet position. However, using VPV/T system leads to gradually decrease in the temperature from the maximum to the minimum temperatures. The local temperature decreases with increasing the wind speed, and VPV/T system shows more uniformity in the temperature distribution compared to the conventional system.

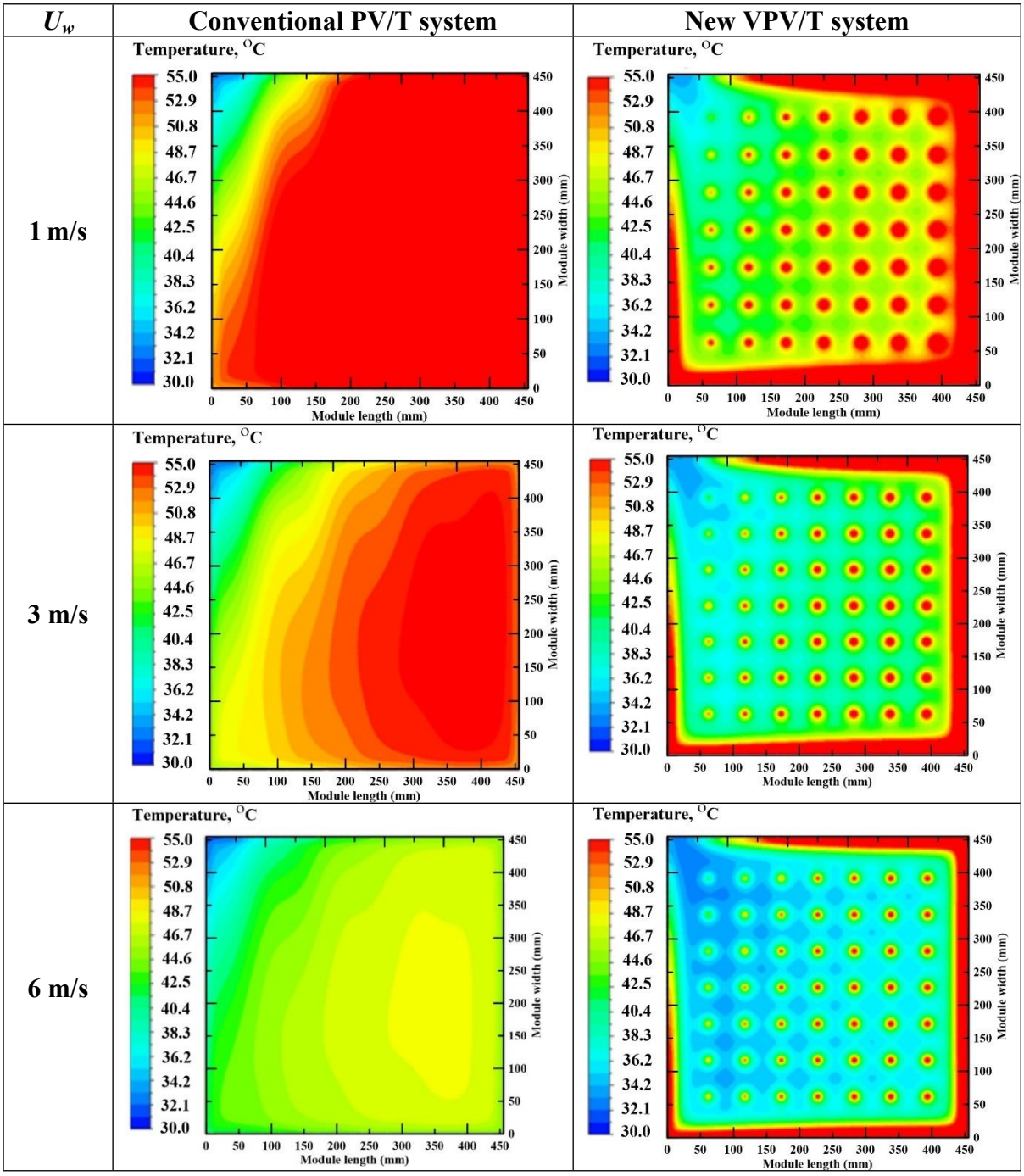

Fig. 9. Local top glass surface temperature for PV at different values of U_w.

Table 4 shows the variation of the difference between the water outlet and inlet temperature at different Re and wind speeds for both designs. It is an evident that the new VPV/T system attained higher coolant rise temperature compared to the conventional PV/T system at the same conditions.

Table 4 variation of $\Delta T = T_{out} - T_{in}$ with Re and U_w for both the conventional PV/T and new VPV/T systems

U_w=2m/s, P_v=0.01Pa			Re=10, P_v=0.01Pa		
Re	$\Delta T = T_{out} - T_{in}$		U_w	$\Delta T = T_{out} - T_{in}$	
	Conventional PV/T	New VPV/T		Conventional PV/T	New VPV/T
10	30.09	57.75	**1**	35.58	61.43
15	28.09	48.47	**2**	30.09	57.75
25	23.89	35.67	**3**	26.03	54.72
75	12.24	14.55	**4**	22.93	52.24
100	9.72	11.17	**5**	20.49	50.24
150	6.86	7.62	**6**	18.54	48.30

4.3. Design parameters for the new VPV/T system

In this section, the effect of different design parameters, namely top EVA emissivity, glass coating emissivity, and air gap vacuum pressure on the performance of vacuum PV/T system is discussed. This section is conducted at Re =10; wind speed of 2 m/s, and solar radiation of 1000 W/m^2 .

4.3.1. Effect of the emissivity coating on the top EVA layer

In VPV/T collector system, the cavity vacuum gap separates the top EVA and the glass layers. The emissivity of the top EVA layer affects the heat transfer from the EVA layer to the glass layer through the vacuum layer. Fig. 10 shows the effect of changing the top EVA layer emissivity of the coating on the average solar cell, maximum solar cell, top glass layer, water outlet temperatures, and thermal and electrical power. In the current section, the emissivity of the EVA layer changes from 0.18 to 0.9 whilst the inner glass layer was coated with L-e coating with an emissivity of 0.18. It is noticed that an average PV temperature slightly decreases with the increase of EVA emissivity, as shown in Fig. 10a. This is because of the enhancement that occurs in the heat transfer from the EVA layer by the increase of the emissivity. However, the difference in the average cell temperature was predicted to be 1.1 ^oC when the emissivity changes

View Article Online
DOI: 10.1039/D0SE01102A

from 0.18 to 0.9. Consequently, the maximum cell temperature decreases with the increase of EVA emissivity as the heat transferred from the layer increases. The top glass layer temperature increases with the increase of EVA emissivity as the heat loss increases and more heat transfer through the glass layer as depicted by Fig. 10c. Water outlet temperature is dependent on the solar cell temperature, so it decreases with the increase of EVA layer emissivity as the solar cell temperature decreases. The thermal and electrical net power variation with the EVA emissivity is shown in Fig. 10d. Thermal power decreases from 62.76 W at $\varepsilon = 0.18$ to 61.31 W at $\varepsilon = 0.9$, and this is due to the decrease in the water outlet temperature. While electrical net power increases from 28.54 W at $\varepsilon = 0.18$ to 28.63 W at $\varepsilon = 0.9$ and this is because of the reduction of solar cell temperature with the increase of the EVA emissivity that leads to an increase in the solar cell efficiency. Based on these results, it is favourable to use the common available EVA layer without further coating for lower cost.

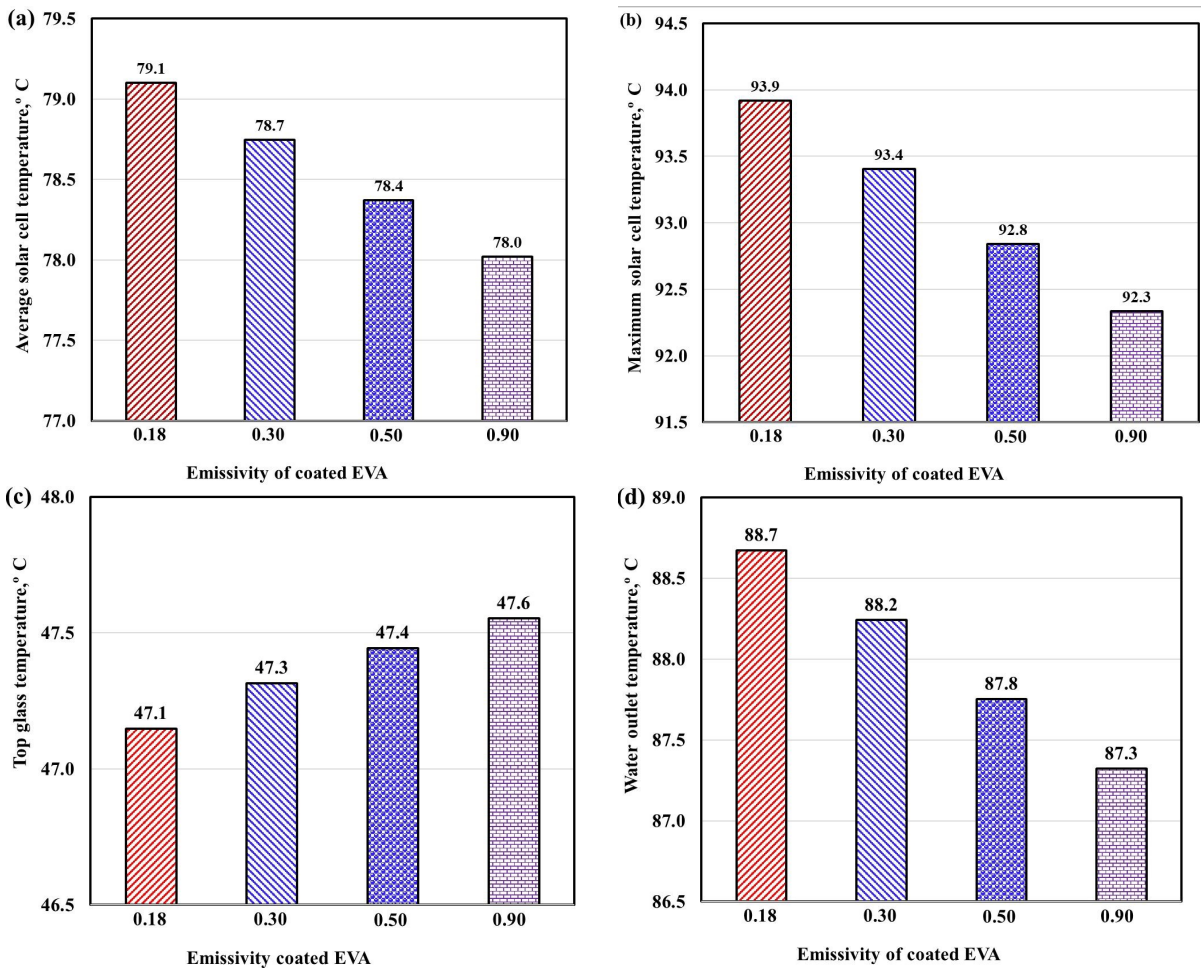

View Article Online
DOI: 10.1039/D0SE01102A

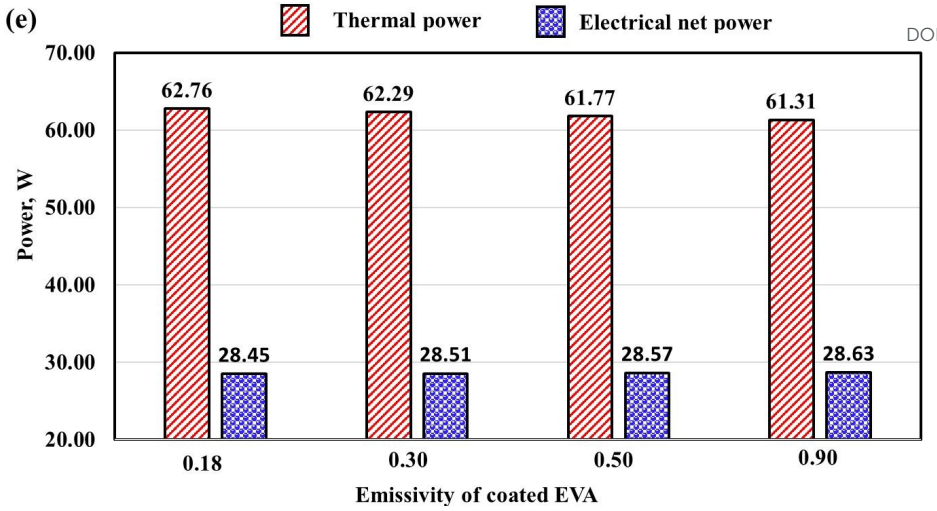

Fig. 10. Variation of a) average PV temperature, b) maximum PV temperature, c) Top glass layer temperature, d) water outlet temperature, and e) Thermal and Electrical power with EVA layer emissivity.

4.3.2. Effect of coating emissivity of the glass cover

The effect of the emissivity of glass side facing the vacuum layer on average solar cell temperature, maximum solar cell temperature, top glass surface layer temperature, water outlet temperature, thermal power, and net electrical power is illustrated in Fig. 11. This simulation is also conducted at EVA emissivity of 0.9, which is cost-effective. The heat loss from the glass layer increases with the increase of the glass surface emissivity and hence decrease the average cell temperature, maximum cell temperature, and water outlet temperature, as shown in Fig. 11a, Fig. 11b, and Fig. 11c, respectively. However, top glass layer temperature increases with the increase of heat loss from the surface that increases with the emissivity. Figure 11e presents the variation of thermal power and electrical net power with the emissivity. The thermal power decreases with the increase of the emissivity as the water out temperature decreases. The net electrical power increases with the increase of emissivity. Therefore, it can be concluded that using an Le coated glass with cost-effective EVA emissivity accomplish higher thermal performance of the VPV/T system.

4.3.3. Effect of vacuum pressure

The heat transfer through the cavity vacuum layer is transferred by radiation and conduction. Figure 12 shows the effect of vacuum pressure on water outlet, average solar cell temperatures, and thermal and electrical net power. The PV temperature decreases with the increase of the cavity vacuum pressure because of increasing of the cavity thermal conductivity of the vacuum layer. Additionally, increasing the vacuum pressure increases the heat loss. Hence, the water

outlet temperature and the PV temperature decrease ith a small value until the vacuum pressure reaches 10 Pa then sharply decrease with an increase of vacuum pressure. It is worth mentioning that a stable performance of the new proposed VPV/T system is attained even with vacuum pressure degradation up to 10 Pa.

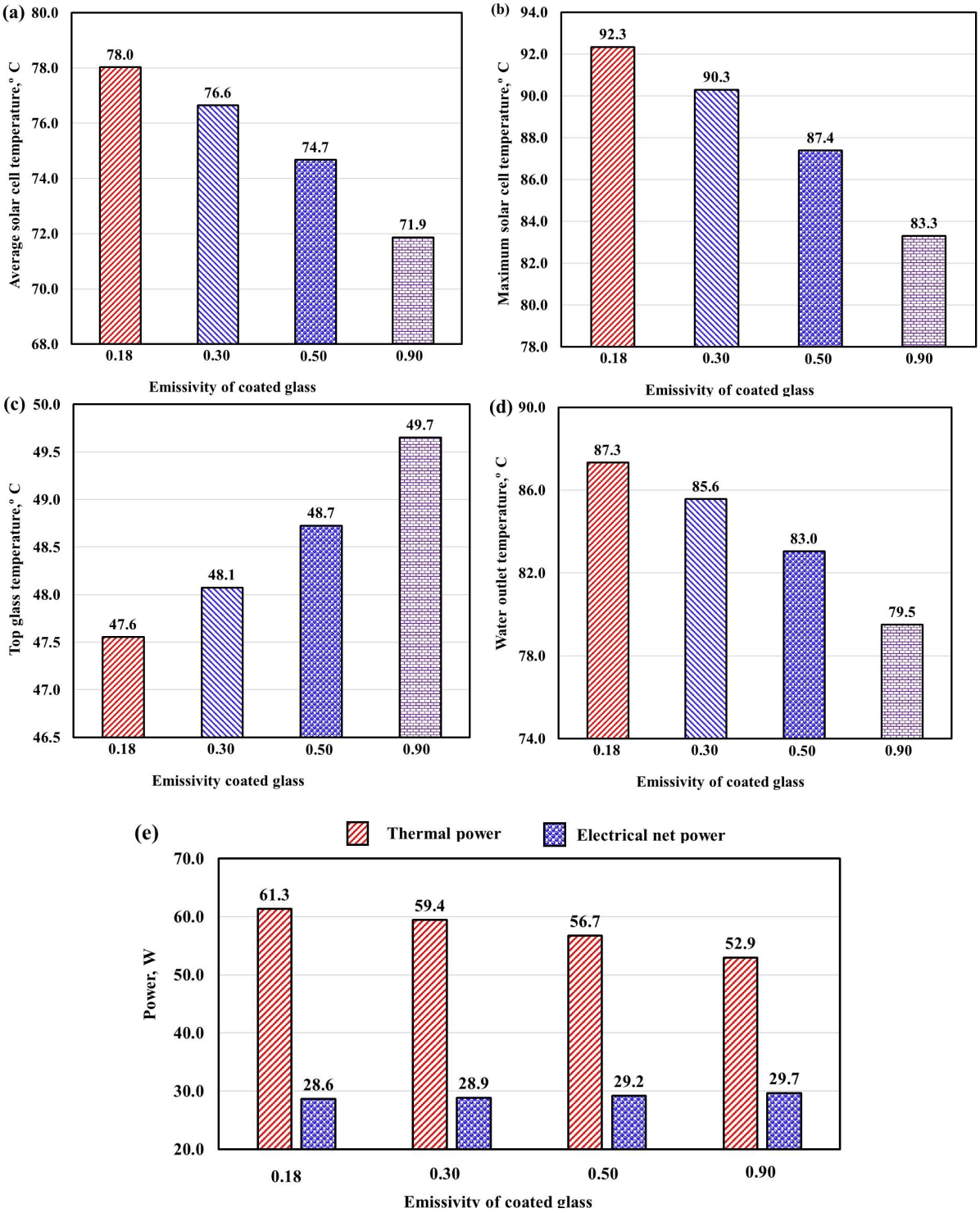

Fig. 11. Variation of a) average PV temperature, b) maximum PV temperature, c) Top surface temperature, d) coolant outlet temperature, and e) thermal and electrical power with glass emissivity

View Article Online
DOI: 10.1039/D0SE01102A

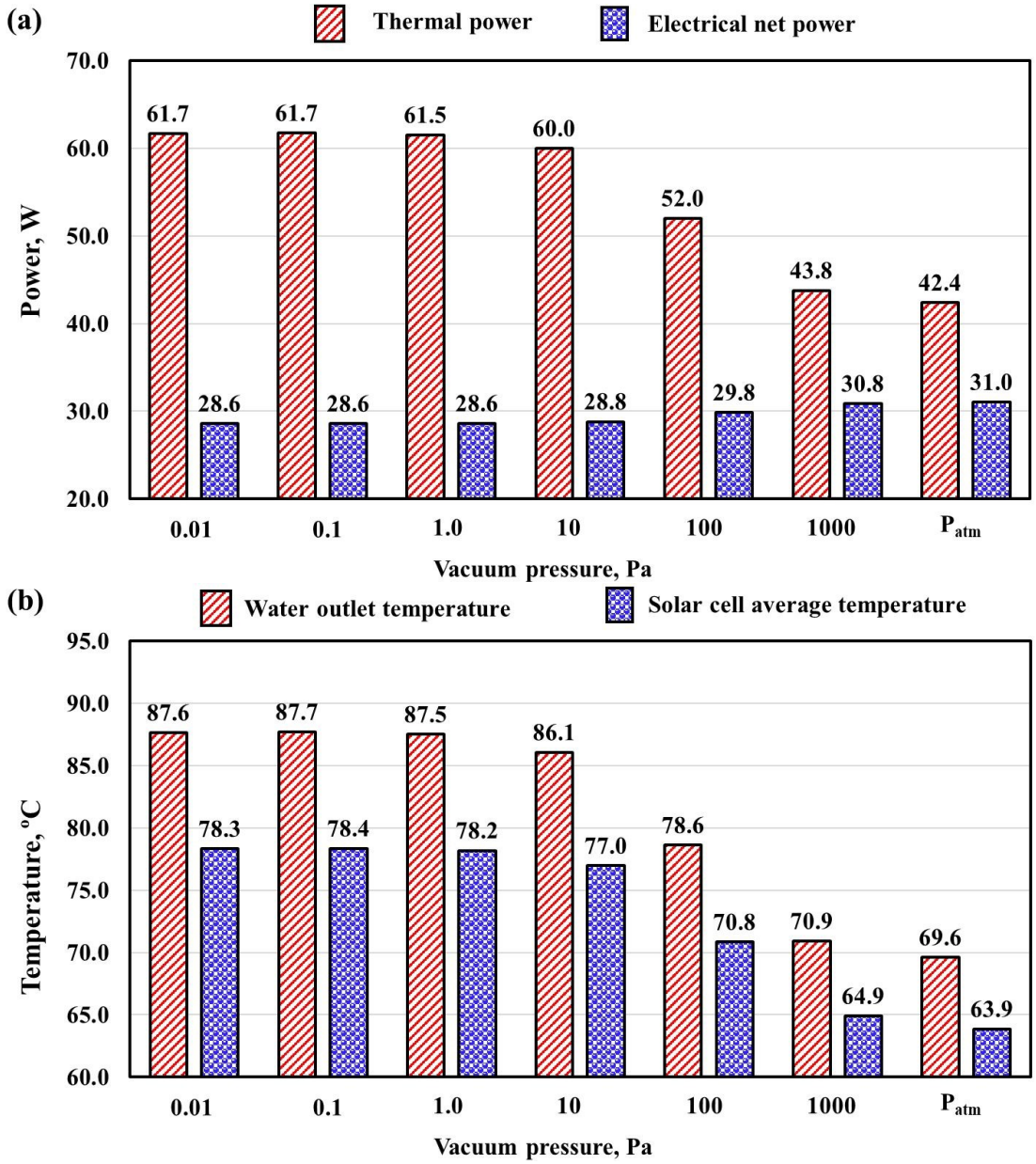

Fig. 12. Variation of a) Thermal and Electrical net power, and b) Water outlet and average solar cell temperatures

The variation of the local top glass layer temperature with the vacuum pressure is presented in Fig. 13. Increasing the vacuum pressure leads to an increase in the local temperature and hence increase the heat loss on the glass layer. In addition, the thermal bridge impact through the pillars and sealing can be highly detected at higher cavity vacuum pressure.

View Article Online
DOI: 10.1039/D0SE01102A

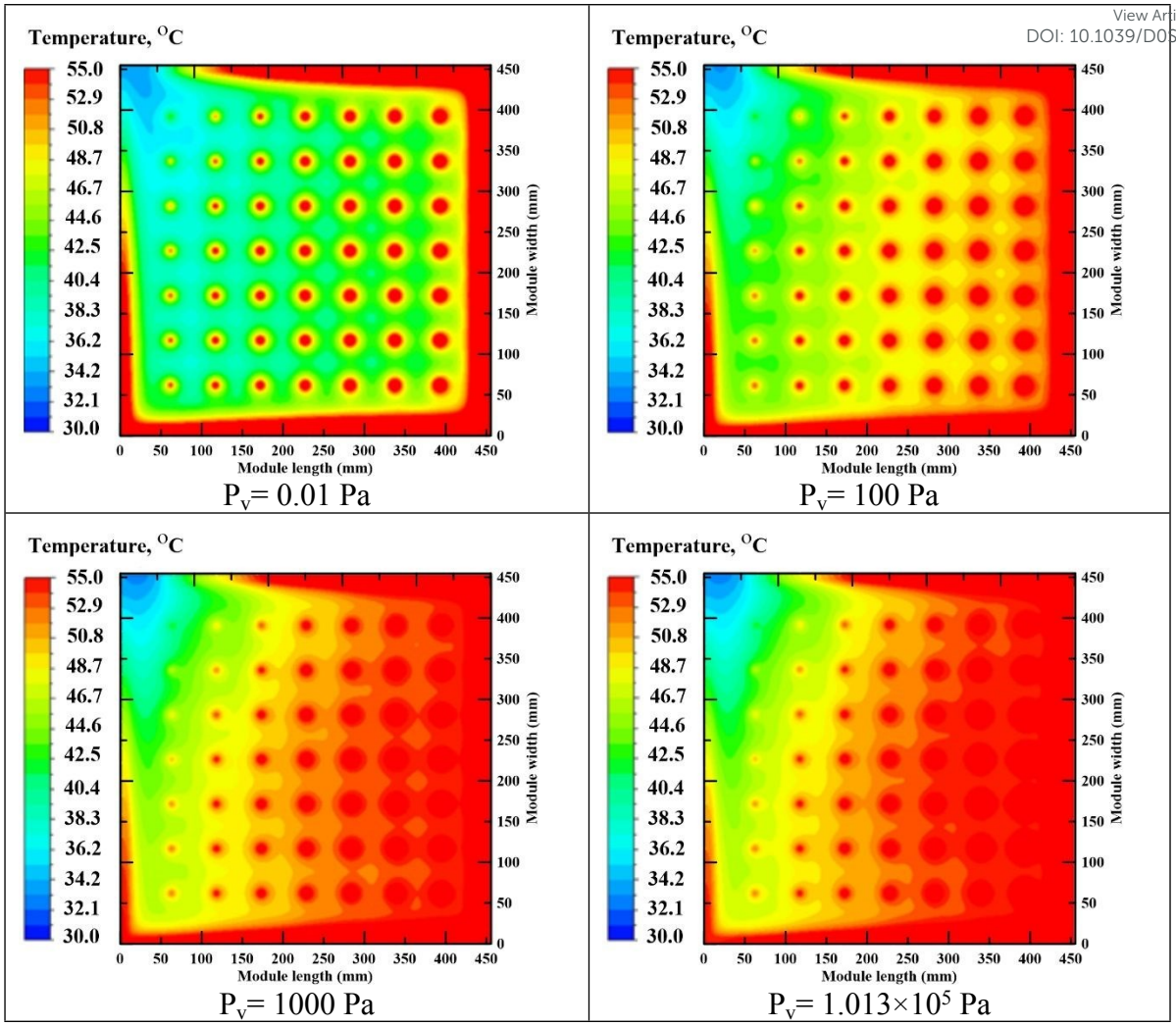

Fig. 13. Local temperature of top glass surface at various cavity vacuum pressure levels.

4.4. Transient analysis of PV/T and VPV/T collectors.

This section gives a comparison between the real instantaneous thermal performance of the conventional PV/T collector system and new proposed VPV/T collector system at the meteorological conditions of Cairo (30.0444° N, 31.2357°), Egypt. The transient simulation is conducted on a typical day for this city on the 10th of July 2019. Fig. 14 shows hourly variation of weather conditions for that day. These data are imported using the transient profile option. This profile is used to estimate updated boundary condition in the transient simulation every hour. The current transient simulation is conducted at Re of 50 where a comparable solar cell temperature for both designs exits with higher thermal energy for the VPV/T collector system.

View Article Online
DOI: 10.1039/D0SE01102A

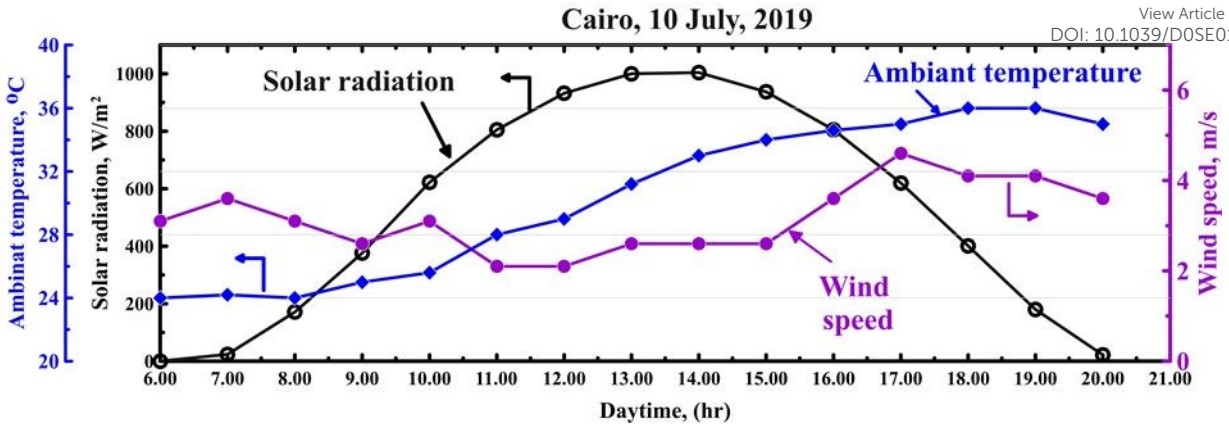

Fig. 14 hourly variation of solar radiation, wind speed, and ambient temperature in a typical day for Cairo (30.0444° N, 31.2357°), Egypt on 10th of July 2019 the most.

Figure 15 provides a transient comparison between new VPV/T system and conventional PV/T system for average solar cell temperature, maximum solar cell temperature, top glass surface temperature, water outlet temperature, and gained thermal power at a vacuum pressure of 0.01 Pa, V_{wind} of 2 m/s and Re of 50. Average PV temperature increases with time due to the increase of solar irradiance, and it reaches its maximum and then decreases again with time. New VPV/T system shows relative similar values to the PV/T during the first three hours of the simulation, and then the difference increases with time until it reaches its maximum and it decreases again with time. The same behaviour is noticed for maximum solar cell temperature and water outlet temperature, as shown in Fig. 15b and Fig. 15d. Top glass surface temperature is lower in the case VPV/T compared to PV/T system Fig. 15c. The gained thermal power is higher in the VPV/T with nearly similar gained electrical power.

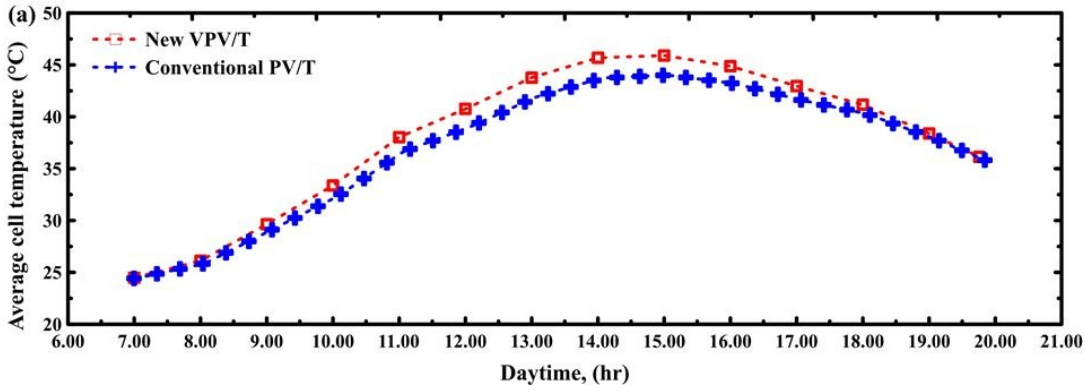

View Article Online
DOI: 10.1039/D0SE01102A

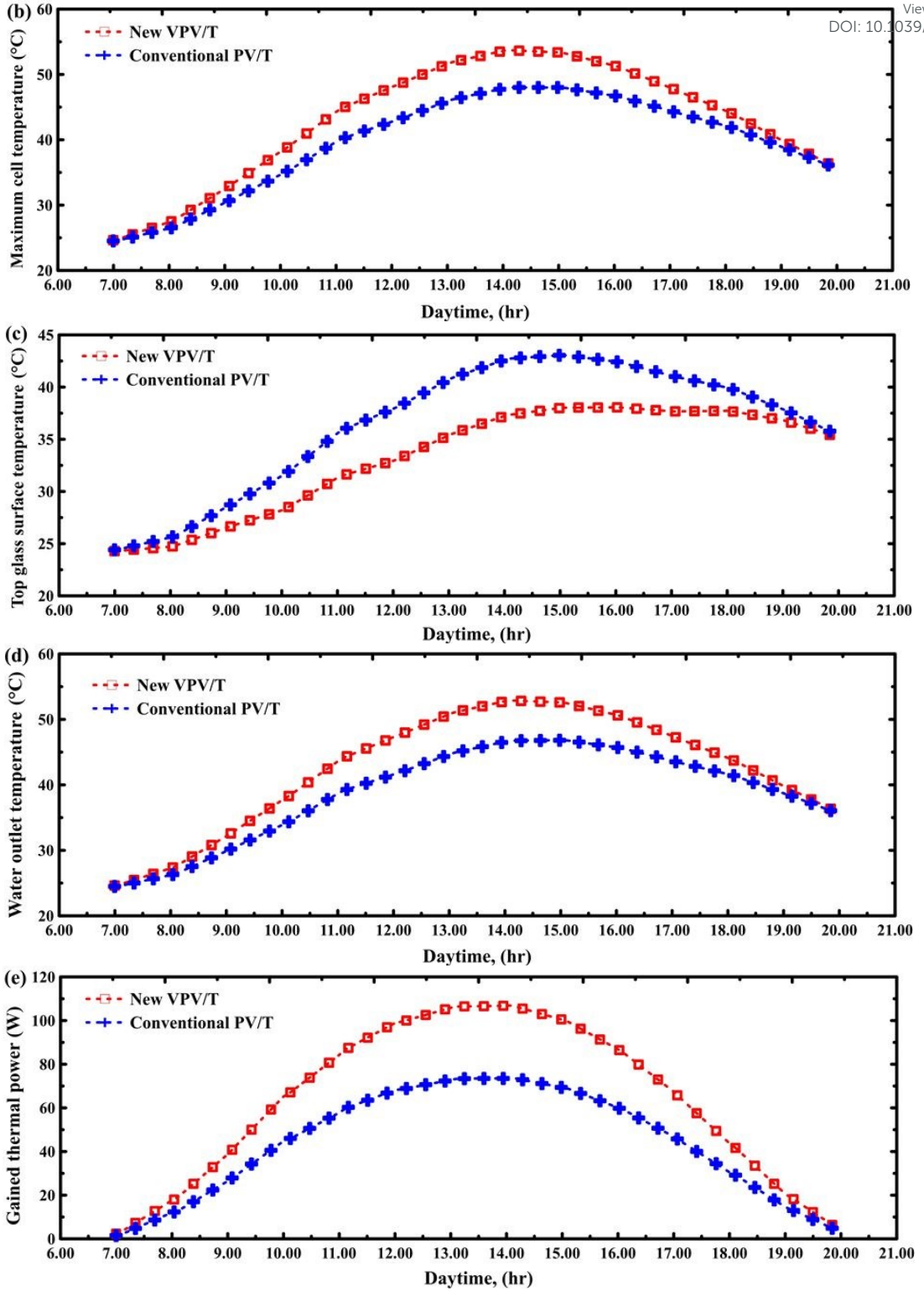

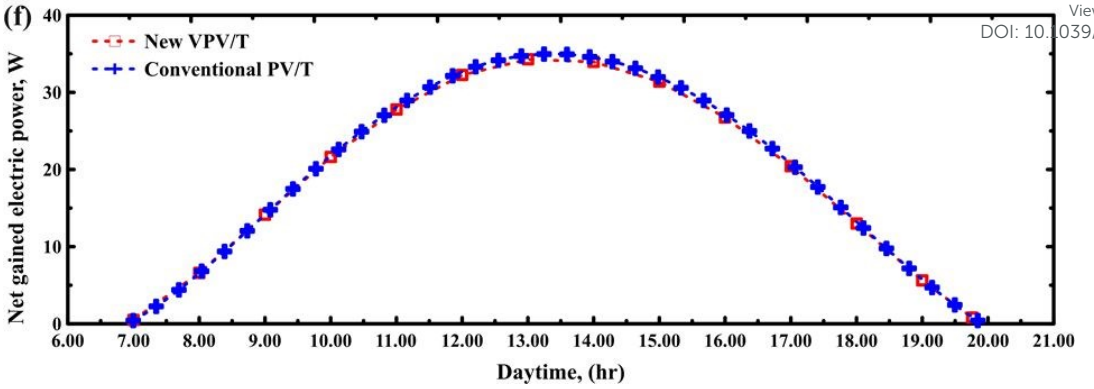

Fig. 15. Transient variation of a) Average PV temperature, b) Maximum PV temperature, c) Top PV temperature, d) Water outlet temperature, e) Gained thermal power and e) net electrical power

4.5. Exergy assessment

Figure 16a shows the variation in the electrical, thermal, and total exergy (*Ex*) of the VPV/T system with Re. As Re increases, both the thermal and electrical exergies improve the total exergy consequently, and both reached at the peak of Re = 50. At high Re values, the thermal exergy is decreased. The considerable reduction is dominant, considered to be a consequence of T_m reduction. A decrease of T_m at high Re occurs because of the smaller temperature difference between the inlet and outlet. Hence, the low-temperature difference produced shallow exergy content. Furthermore, the improved electrical exergy led to low-grade heat energy. The maximum total exergy of the VPV/T system is about 78 W which is attained at Re = 50. While with increasing Re, the amount of heat transfer to the coolant increases. This trend is shown by the conventional PV/T, as shown in Fig. 16b. When the VPV/T is compared to conventional PV/T, it is evident that a 33.6 % improve in the total exergy content can be accomplished by using the VPV/T at the lowest Re = 10. Besides, the total exergy content is improved by approximately 5.8 % at the highest Re value of 150. Furthermore, the electrical, thermal, and total exergy efficiencies for both designs are shown in Fig. 16c and Fig. 16d, respectively. It is evident that the maximum overall exergy efficiency obtained at the highest investigated Re of 150. The maximum total exergy efficiency values are predicted to be 38.01% and 35.91% for VPV/T and PV/T collector system designs, respectively. Other exergy results at different wind speed are displayed in the supplementary data file.

View Article Online
DOI: 10.1039/D0SE01102A

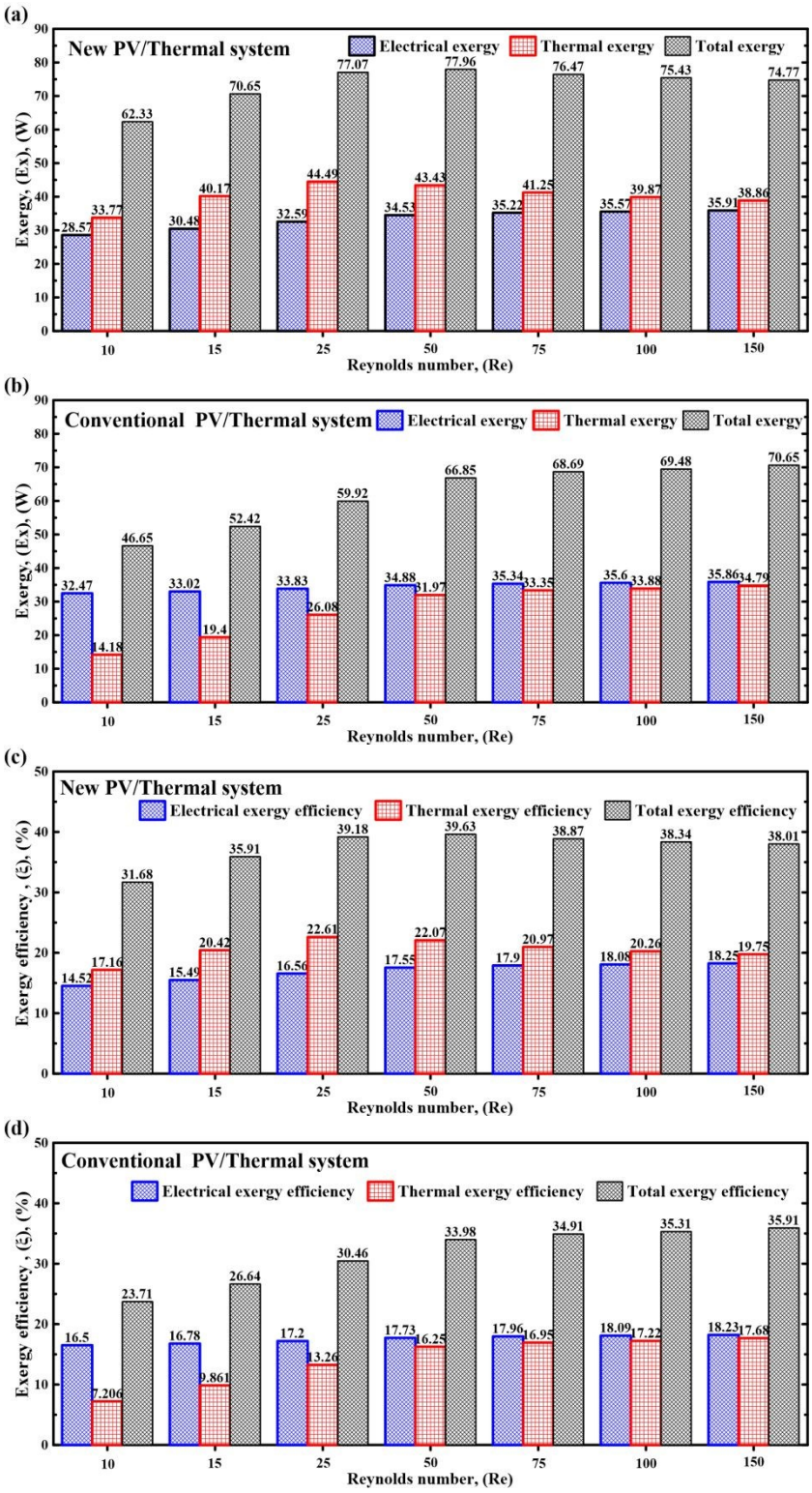

Fig. 16 Variation of (a) VPV/T system exergy (b) conventional PV/T system exergy (c) VPV/T system exergy efficiency (b) conventional PV/T system exergy efficiency different Re.

View Article Online
DOI: 10.1039/D0SE01102A

5. Conclusions

In the present study, a new composited edge sealed vacuum glazed photovoltaic thermal (VPV/T) solar collector system is proposed. This design is compared with the conventional PV/T module. Using a 3D validated thermal model. Major conclusions are summarised into the following points.

1- The VPV/T module attained higher outlet water temperature and consequently, higher thermal energy gain compared to the conventional PV/T system over the investigated Re numbers.
2- At Re greater than 60 and solar radiation of 1000W/m^2, the gained electrical and thermal power from the VPV/T design is higher than the conventional VPV/T system at the same conditions.
3- The VPV/T gained thermal energy is much higher than the conventional PV/T system even at higher wind speed. For instance, at a wind speed of 5 m/s and Re of 10, the gained thermal energy for the PV/T and the new VPV/T system is 22 W and 53W, respectively. Around 140% enhancement in the thermal energy gain was accomplished while the electrical power is slightly changed from 33.7 W to 29.3W for the PV/T and the VPV/T, respectively.
4- Stable thermal performance of the VPV/T module is accomplished on a wide range of vacuum pressure up to 1 Pa.
5- Based on the exergy analysis, the new VPV/T achieved higher total exergy efficiency up to 40 % at Re of 40 while it was around 33% for the conventional PV/T system.

A serpentine flow filed heat sink is used in this study. This design was selected based on recent studies that used sheet and tube serpentine thermal absorber. However, the contact between the tube surface and the sheets causes a big problem in the heat transfer and CFD meshing of this thermal absorber. Therefore, a wide channel with serpentine flow filed is used. However, the temperature difference across the silicon wafer still high specially at lower Re. Therefore, it is recommended as a future investigation to use different designs of thermal absorbers with shorter flow path to accomplish better silicon wafer temperature uniformity. In addition, the performance of both conventional PV/T and VPV/T systems should be also discovered at various ambient temperature, solar radiation levels and various heat sink designs in the future studies.

Nomenclatures

C_p	specific heat J/kg.K
E	rate of exergy per unit area [W/m^2]
Ex	exergy [w]
G	solar radiation [W/m^2]
D_h	channel hydraulic diameter [m]
h	heat transfer coefficient [W/m^{2}K]
H	channel height [m]
K	thermal conductivity [W/m.K]
l	thickness [m]
$\dot{m}$	mass flowrate [kg/s]
P	pressure [Pa]

View Article Online
DOI: 10.1039/D0SE01102A

P	power [W]
R	reflectivity [--]
Re	Reynolds number [--]
T	temperature [K]
t	time [s]
U	velocity in x [m/s]
V	velocity in y [m/s]
W	velocity in z [m/s], channel width [m]

Greek symbols

α	absorptivity [--]
ε	emissivity [--]
ρ	density [kg/m^3]
τ	transmissivity
μ	dynamic viscosity [Pa.s]
η	efficiency [--]
Ψ_s	coefficient of radiation exergy [--]
ξ	exergy Efficiency [--]

Subscript

A	ambient
el	electrical
f	fluid
g	glass
in	inlet
out	outlet
sc	solar Cell
sol	solar
ch	channel
th	thermal
ref	reference

References

[1] Ju X, Xu C, Hu Y, Han X, Wei G, Du X. A review on the development of photovoltaic/concentrated solar power (PV-CSP) hybrid systems. Sol Energy Mater Sol Cells 2017;161:305–27. https://doi.org/https://doi.org/10.1016/j.solmat.2016.12.004.

[2] Daneshazarian R, Cuce E, Cuce PM, Sher F. Concentrating photovoltaic thermal (CPVT) collectors and systems: Theory, performance assessment and applications. Renew Sustain Energy Rev 2018;81:473–92. https://doi.org/10.1016/j.rser.2017.08.013.

[3] Ji Y, Xu Q, Riggs B, Islam K, Ollanik A, Ermer JH, et al. Optical Design and Validation of an Infrared Transmissive Spectrum Splitting Concentrator Photovoltaic Module 2017;7:1469–78.

[4] Wu G, Yang Q, Zhang Y, Fang H, Feng C, Zheng H. Energy and optical analysis of photovoltaic thermal integrated with rotary linear curved Fresnel lens inside a Chinese solar greenhouse. Energy 2020;197:117215. https://doi.org/https://doi.org/10.1016/j.energy.2020.117215.

[5] Rahman MM, Hasanuzzaman M, Rahim NA. Effects of operational conditions on the energy efficiency of photovoltaic modules operating in Malaysia. J Clean Prod 2017.

View Article Online
DOI: 10.1039/D0SE01102A

https://doi.org/10.1016/j.jclepro.2016.12.029.

[6] Dubey S, Tiwari GN. Thermal modeling of a combined system of photovoltaic thermal (PV/T) solar water heater. Sol Energy 2008;82:602–12. https://doi.org/10.1016/j.solener.2008.02.005.

[7] Sultan SM, Ervina Efzan MN. Review on recent Photovoltaic/Thermal (PV/T) technology advances and applications. Sol Energy 2018;173:939–54. https://doi.org/10.1016/j.solener.2018.08.032.

[8] Barone G, Buonomano A, Forzano C, Palombo A, Panagopoulos O. Photovoltaic thermal collectors: Experimental analysis and simulation model of an innovative low-cost water-based prototype. Energy 2019;179:502–16. https://doi.org/https://doi.org/10.1016/j.energy.2019.04.140.

[9] Pang W, Cui Y, Zhang Q, Wilson GJ, Yan H. A comparative analysis on performances of flat plate photovoltaic/thermal collectors in view of operating media, structural designs, and climate conditions. Renew Sustain Energy Rev 2020;119:109599. https://doi.org/10.1016/j.rser.2019.109599.

[10] Fuentes M, Vivar M, de la Casa J, Aguilera J. An experimental comparison between commercial hybrid PV-T and simple PV systems intended for BIPV. Renew Sustain Energy Rev 2018;93:110–20. https://doi.org/10.1016/j.rser.2018.05.021.

[11] Hemmat Esfe M, Kamyab MH, Valadkhani M. Application of nanofluids and fluids in photovoltaic thermal system: An updated review. Sol Energy 2020. https://doi.org/10.1016/j.solener.2020.01.015.

[12] Ahmad L, Khordehgah N, Malinauskaite J, Jouhara H. Recent advances and applications of solar photovoltaics and thermal technologies. Energy 2020;207:118254. https://doi.org/https://doi.org/10.1016/j.energy.2020.118254.

[13] Khanjari Y, Pourfayaz F, Kasaeian AB. Numerical investigation on using of nanofluid in a water-cooled photovoltaic thermal system. Energy Convers Manag 2016;122:263–78. https://doi.org/10.1016/j.enconman.2016.05.083.

[14] Sardarabadi M, Passandideh-Fard M, Zeinali Heris S. Experimental investigation of the effects of silica/water nanofluid onPV/T (photovoltaic thermal units). Energy 2014;66:264–72. https://doi.org/10.1016/j.energy.2014.01.102.

[15] Hassani S, Saidur R, Mekhilef S, Taylor RA. Environmental and exergy benefit of nanofluid-based hybrid PV/T systems. Energy Convers Manag 2016;123:431–44. https://doi.org/10.1016/j.enconman.2016.06.061.

[16] Ahmed M, Radwan A. Performance evaluation of new modified low-concentrator polycrystalline silicon photovoltaic/thermal systems. Energy Convers Manag 2017;149:593–607. https://doi.org/http://dx.doi.org/10.1016/j.enconman.2017.07.057.

[17] Sopian K, Yigit KS, Liu HT, Kakaç S, Veziroglu TN. Performance analysis of photovoltaic thermal air heaters. Energy Convers Manag 1996. https://doi.org/10.1016/0196-8904(96)00010-6.

[18] Nahar A, Hasanuzzaman M, Rahim NA. Numerical and experimental investigation on the performance of a photovoltaic thermal collector with parallel plate flow channel under different operating conditions in Malaysia. Sol Energy 2017;144:517–28. https://doi.org/https://doi.org/10.1016/j.solener.2017.01.041.

[19] Harb AE-MA, Radwan A, Elsayed K, Sedrak M, Ahmed M. Influence of varying the Ethylene-Vinyl Acetate layer thicknesses on the performance of a polycrystalline silicon solar cell integrated with a microchannel heat sink. Sol Energy 2020;195:592–609. https://doi.org/https://doi.org/10.1016/j.solener.2019.11.082.

[20] Pang W, Zhang Q, Cui Y, Zhang L, Yu H, Zhang X, et al. Numerical simulation and experimental validation of a photovoltaic/thermal system based on a roll-bond aluminum collector. Energy 2019;187:115990. https://doi.org/https://doi.org/10.1016/j.energy.2019.115990.

[21] Arya F, Moss R, Hyde T, Shire S, Henshall P, Eames P. Vacuum enclosures for solar thermal panels Part 1: Fabrication and hot-box testing. Sol Energy 2018;174:1212–23. https://doi.org/https://doi.org/10.1016/j.solener.2018.10.064.

[22] Memon S, Fang Y, Eames PC. The influence of low-temperature surface induction on evacuation, pump-out hole sealing and thermal performance of composite edge-sealed vacuum insulated glazing. Renew Energy 2019;135:450–64. https://doi.org/10.1016/j.renene.2018.12.025.

[23] Memon S, Farukh F, Eames PC, Silberschmidt V V. A new low-temperature hermetic composite edge seal for the fabrication of triple vacuum glazing. Vacuum 2015;120:73–82. https://doi.org/https://doi.org/10.1016/j.vacuum.2015.06.024.

[24] Memon S. Experimental measurement of hermetic edge seal's thermal conductivity for the thermal transmittance prediction of triple vacuum glazing. Case Stud Therm Eng 2017;10:169–78. https://doi.org/https://doi.org/10.1016/j.csite.2017.06.002.

[25] Jayakumar JS, Mahajani SM, Mandal JC, Vijayan PK, Bhoi R. Experimental and CFD estimation of heat transfer in helically coiled heat exchangers. Chem Eng Res Des 2008;86:221–32. https://doi.org/10.1016/j.cherd.2007.10.021.

[26] Siddiqui MU, Arif a. FM. Electrical, thermal and structural performance of a cooled PV module: Transient analysis using a multiphysics model. Appl Energy 2013;112:300–12. https://doi.org/10.1016/j.apenergy.2013.06.030.

[27] Ren X, Yu M, Zhao X, Li J, Zheng S, Chen F, et al. Assessment of the cost reduction potential of a novel loop-heat-pipe solar photovoltaic/thermal system by employing the distributed parameter model. Energy 2020;190:116338. https://doi.org/https://doi.org/10.1016/j.energy.2019.116338.

[28] Xu Z, Kleinstreuer C. Concentration photovoltaic-thermal energy co-generation system using nanofluids for cooling and heating. Energy Convers Manag 2014;87:504–12. https://doi.org/10.1016/j.enconman.2014.07.047.

[29] Zhou J, Yi Q, Wang Y, Ye Z. Temperature distribution of photovoltaic module based on finite element simulation. Sol Energy 2015;111:97–103. https://doi.org/10.1016/j.solener.2014.10.040.

[30] ANSYS FLUENT Theory Guide 2011.

[31] Kwon JS, Jang CH, Jung H, Song TH. Effective thermal conductivity of various filling materials for vacuum insulation panels. Int J Heat Mass Transf 2009;52:5525–32. https://doi.org/10.1016/j.ijheatmasstransfer.2009.06.029.

[32] Fang Y, Hyde T, Hewitt N, Eames PC, Norton B. Comparison of vacuum glazing thermal performance predicted using two- and three-dimensional models and their

View Article Online
DOI: 10.1039/D0SE01102A

experimental validation. Sol Energy Mater Sol Cells 2009;93:1492–8. https://doi.org/https://doi.org/10.1016/j.solmat.2009.03.025.

[33] Kim J, Song TH. Vacuum insulation properties of glass wool and opacified fumed silica under variable pressing load and vacuum level. Int J Heat Mass Transf 2013;64:783–91. https://doi.org/10.1016/j.ijheatmasstransfer.2013.05.012.

[34] Teo HGG, Lee PSS, Hawlader MN a. N a. An active cooling system for photovoltaic modules. Appl Energy 2012;90:309–15. https://doi.org/10.1016/j.apenergy.2011.01.017.

[35] El-Samie MMA, Ju X, Zhang Z, Adam SA, Pan X, Xu C. Three-dimensional numerical investigation of a hybrid low concentrated photovoltaic/thermal system. Energy 2020;190:116436. https://doi.org/https://doi.org/10.1016/j.energy.2019.116436.

[36] Emam M, Ahmed M. Performance analysis of a new concentrator photovoltaic system integrated with phase change material and water jacket. Sol Energy 2018;173:1158–72. https://doi.org/https://doi.org/10.1016/j.solener.2018.08.069.

[37] Evola G, Marletta L. Exergy and thermoeconomic optimization of a water-cooled glazed hybrid photovoltaic/thermal (PVT) collector. Sol Energy 2014;107:12–25. https://doi.org/10.1016/j.solener.2014.05.041.

[38] Hosseinzadeh M, Sardarabadi M, Passandideh-Fard M. Energy and exergy analysis of nanofluid based photovoltaic thermal system integrated with phase change material. Energy 2018;147:636–47. https://doi.org/https://doi.org/10.1016/j.energy.2018.01.073.

[39] Zimmermann S, Helmers H, Tiwari MK, Paredes S, Michel B, Wiesenfarth M, et al. A high-efficiency hybrid high-concentration photovoltaic system. Int J Heat Mass Transf 2015;89:514–21. https://doi.org/10.1016/j.ijheatmasstransfer.2015.04.068.

[40] Jeter SM. Maximum conversion efficiency for the utilization of direct solar radiation. Sol Energy 1981;26:231–6. https://doi.org/10.1016/0038-092X(81)90207-3.

[41] Radwan A, Ahmed M. The influence of microchannel heat sink configurations on the performance of low concentrator photovoltaic systems. Appl Energy 2017;206:594–611. https://doi.org/10.1016/j.apenergy.2017.08.202.

[42] Joshi ASS, Tiwari a., Tiwari GNN, Dincer I, Reddy BV V. Performance evaluation of a hybrid photovoltaic thermal (PV/T) (glass-to-glass) system. Int J Therm Sci 2009;48:154–64. https://doi.org/10.1016/j.ijthermalsci.2008.05.001.

[43] El M, Slimani A, Amirat M, Kurucz I, Bahria S, Hamidat A, et al. A detailed thermal-electrical model of three photovoltaic / thermal (PV / T) hybrid air collectors and photovoltaic (PV) module : Comparative study under Algiers climatic conditions. Energy Convers Manag 2017;133:458–76. https://doi.org/10.1016/j.enconman.2016.10.066.

[44] Rohsenow WM, Hartnett JRPR, Cho YI. Forced convection internal flow in ducts. New York: McGraw-Hill; 1998.